

1 **Diagnostic computation of moisture budgets in the**
2 **ERA-Interim Reanalysis with reference to analysis of**
3 **CMIP-archived atmospheric model data**

4 RICHARD SEAGER AND NAOMI HENDERSON *

Lamont Doherty Earth Observatory of Columbia University, Palisades, New York

* *Corresponding author address:* Richard Seager, Lamont Doherty Earth Observatory of Columbia University, 61 Route 9W., Palisades, NY 10964. Email: seager@ldeo.columbia.edu

To be submitted to *Journal of Climate* November 2012. LDEO Contribution Number xxxx.

ABSTRACT

5
6 The diagnostic evaluation of moisture budgets in archived atmosphere model data is exam-
7 ined. Sources of error in diagnostic computation can arise from use of numerical methods
8 that are different to those used in the atmosphere model, the time and vertical resolution
9 of the archived data and data availability. These sources of error are assessed using the cli-
10 matological moisture balance in the European Centre for Medium Range Weather Forecasts
11 Interim Reanalysis (ERA-I) which archives vertically integrated moisture fluxes and conver-
12 gence. The largest single source of error arises from the diagnostic evaluation of divergence
13 with the chosen second order accurate centered finite difference scheme applied to the actual
14 vertically integrated moisture fluxes leading to significant differences from the actual moisture
15 convergence. Using daily instead of 6 hourly data leads to an underestimation of the patterns
16 of moisture divergence and convergence by mid-latitude transient eddies. An even larger and
17 more widespread source of error comes from reducing the vertical resolution of the model
18 data to the 8 levels typical of data archived for the Coupled Model Intercomparison Project
19 (CMIP). Dividing moisture divergence into components due to the divergent flow and advec-
20 tion requires bringing the divergence operator inside the vertical integral which introduces a
21 surface term for which a means of accurate evaluation is developed. The analysis of errors is
22 then extended to the case of the spring 1993 Mississippi Valley floods, the causes of which are
23 discussed. For future archiving of data (e.g. by CMIP) it is recommended that monthly means
24 of time step resolution flow-humidity co-variances be archived at high vertical resolution.

1. Introduction

Droughts and floods are some of the main disruptors of human life causing a never ending sequence of death, destruction, suffering, hunger, disease and economic disruption or even collapse (see references in Cutter et al. (2009)). To date almost all of this has been caused by natural climate variations whereby changes in atmospheric circulation and water vapor transports and convergence or divergence create precipitation anomalies that either deprive areas of water or cause an excess. As climate change driven by rising greenhouse gases proceeds, there will be additional hazards caused by both changes in the natural variability, and changes in the mean precipitation distributions, as some tropical and mid-to-high latitude areas get wetter and subtropical dry areas get drier and expand (Allen and Ingram 2002; Held and Soden 2006; Intergovernmental Panel on Climate Change 2007; Seager et al. 2010b, 2012). As for naturally occurring droughts and floods, changes in the mean precipitation distribution are caused by changes in the transport of water vapor in the atmosphere. That is, the atmospheric branch of the hydrological cycle is the key phenomena where these risks to human livelihood originate.

Humans, being naturally curious, have long sought to determine the causes of droughts, pluvials and floods relating them to the responsible changes in atmospheric circulation and water vapor transports. However, ultimately, we need to attempt to anticipate such events in advance so that preparations can be made and the worst impacts avoided. This is true both for the case of natural events occurring on the daily to decadal timescale and also for the more slowly evolving effect of hydroclimate change. In both cases, prediction or projection depends on the use of numerical climate models. Understanding then comes into play as a means of assessing how reliable predictions and projections are, given the fidelity with which the models simulate the important processes. For example, drought over southern North America during La Niña events fundamentally depends on moisture divergence anomalies caused by mean flow anomalies (Seager et al. 2005; Seager and Naik 2012) with the latter tightly coupled to changes in the North Pacific storm track (Seager et al. 2010a; Harnik et al. 2010). In this case, analysis of the moisture budget during El Niño-Southern Oscillation (ENSO) cycles indicates what key features of atmospheric circulation adjustment to tropical Pacific sea surface

54 temperature (SST) anomalies a model needs to simulate in order to effect a useful prediction.

55 Understanding of the causes of floods and droughts and of ongoing hydroclimate change
56 requires a detailed analysis of the atmospheric moisture budget and the linking of this to
57 changes in the atmospheric circulation and, ultimately, the atmospheric and planetary energy
58 budget. This is not very easy to do either in atmospheric models or gridded, model-based, re-
59 analyses of atmospheric observations. In both cases, the models numerically integrate forward
60 a moisture equation designed to best conserve moisture and to preserve a balance between
61 precipitation, P , surface evaporation, E , and the vertically integrated moisture convergence
62 although, in the case of reanalyses, the moisture field is also constrained, directly or indirectly,
63 by observations. However analyses of the causes of hydroclimate variability and change are
64 done diagnostically, after the model has run, using saved data from the model. Typically this
65 data includes velocities and specific humidity on a three dimensional spatial grid as well as
66 surface pressure, P and E . The data may be saved at 6-hourly, daily or monthly temporal
67 resolution, but never at the time step of the model, and only rarely are monthly means of co-
68 variances between quantities (themselves evaluated variously using time step, four times daily,
69 daily mean data etc.) saved. Also the data is only sometimes saved on the native model grid
70 and has often been interpolated to standard pressure levels with varying degrees of vertical
71 resolution.

72 The task of the researcher is to analyze the causes of hydroclimatic events using these
73 incomplete model data sets. At the simplest level the researcher will then discover that the
74 model reported $P - E$ cannot be made to balance the convergence of the vertically integrated
75 moisture flux, no matter how the latter is calculated. However, even if it did balance, this
76 would not be very enlightening. The main goal of such work is to go further and determine
77 what the causes of the moisture convergence or divergence anomalies are and, therefore, break
78 it down into components due to changes in mean circulation, specific humidity and transient
79 eddies (e.g. Seager et al. (2010b); Seager and Naik (2012); Seager et al. (2012); Nakamura
80 et al. (2012)). To do this requires further analysis of the moisture budget and creates a new
81 set of problems as we shall see.

82 The point of this paper is to provide a detailed and thorough assessment of the errors
83 introduced in diagnostic analyses of the moisture budget and how these depend on the temporal

84 and spatial resolution of the data and what additional errors are introduced in attempts to
85 break down moisture convergence into constituent parts. We also aim to provide guidance as
86 to the best possible way to numerically evaluate the moisture budget with existing model data
87 and suggest improvements for the archiving of model and reanalysis data in the future that
88 will allow improved accuracy in diagnostic computations. To this effect we will consider both
89 the climatological moisture budget and the anomalous budget during the Mississippi floods of
90 late spring-early summer 1993.

91 **2. Reanalyses data used**

92 For demonstration purposes we use the European Centre for Medium Range Weather
93 Forecasts (ECMWF) Interim Reanalysis (ERA-I) (Dee et al. 2011) which is the latest of
94 the ECMWF Reanalyses. ERA-I covers the post 1979 period. It assimilates cloud and rain-
95 affected satellite irradiances and has a greatly improved representation of the hydrological cycle
96 relative to its precursor, ERA-40. This makes it good for our purpose. Also ERA-I provides
97 the divergence of the vertically integrated moisture transport as data output, i.e. this provides
98 the actual value of the quantity we are trying to evaluate diagnostically from archived model or
99 reanalysis data. However, it should be noted, because of the assimilation scheme this quantity
100 does not balance the ERA-I $P - E$, even after accounting for the change over time of the
101 vertically integrated specific humidity (see Trenberth et al. (2011)). The original ERA-I data
102 is reported on 37 model levels which are ... We use the 1,5 degree longitude by latitude data.

103 **3. Diagnostic computation of the moisture budget in at-** 104 **mosphere models**

105 Most models use a terrain-following vertical co-ordinate. The σ -coordinate, with $p = \sigma p_s$,
106 where p = pressure and p_s its surface values, was the first such coordinate but more commonly
107 used today is a hybrid vertical coordinate, ξ , which preserves $\xi = 0$ at $p = 0$ and $\xi = 1$ at
108 $p = p_s$ but with the pressure at model level k , p_k , given by $p_k = A_k + B_k p_s$ where A_k and

109 B_k are constants. The hybrid vertical coordinate is usually set up to vary from a terrain-
 110 following coordinate in the lower troposphere to a p coordinate in the stratosphere. On the
 111 other hand model data is commonly archived on standard pressure levels necessitating the use
 112 of a p coordinate in diagnostic analysis. To deal with both these vertical coordinate systems
 113 we begin with a generalized vertical coordinate, η (see Konor and Arakawa (1997)), for which
 114 the material derivative of a quantity is given by:

$$\frac{D}{Dt} = \left(\frac{\partial}{\partial t} \right)_{\eta} + \mathbf{u} \cdot \nabla_{\eta} + \dot{\eta} \frac{\partial}{\partial \eta} \quad (1)$$

115 where $\dot{\eta} = D\eta/Dt$.

116 In this vertical coordinate the moisture equation is (dropping η subscripts):

$$\frac{\partial q}{\partial t} + \nabla \cdot (\mathbf{u}q) + \dot{\eta} \frac{\partial q}{\partial \eta} = e - c \quad (2)$$

117 where q is specific humidity and \mathbf{u} is the velocity vector along η surfaces and e and c are
 118 evaporation and condensation. We use spherical coordinates so the divergence of moisture is
 119 given by:

$$\nabla \cdot (\mathbf{u}q) = \frac{1}{a \cos \phi} \left(\frac{\partial(uq)}{\partial \lambda} + \frac{\partial(vq \cos \phi)}{\partial \phi} \right), \quad (3)$$

120 where u and v are the zonal and meridional components of velocity, a is the radius of the
 121 Earth, λ is longitude and ϕ is latitude. The continuity equation is:

$$\frac{\partial}{\partial t} \frac{\partial p}{\partial \eta} + \nabla \cdot \left(\mathbf{u} \frac{\partial p}{\partial \eta} \right) + \frac{\partial}{\partial \eta} \left(\dot{\eta} \frac{\partial p}{\partial \eta} \right) = 0. \quad (4)$$

122 These can be combined into the flux form of the humidity equation:

$$\frac{\partial}{\partial t} \left(q \frac{\partial p}{\partial \eta} \right) + \nabla \cdot \left(\mathbf{u} q \frac{\partial p}{\partial \eta} \right) + \frac{\partial}{\partial \eta} \left(q \dot{\eta} \frac{\partial p}{\partial \eta} \right) = \frac{\partial p}{\partial \eta} (e - c) \quad (5)$$

123 This equation can be vertically integrated to derive a relation for the precipitation minus
 124 surface evaporation $P - E$:

$$P - E = -\frac{1}{g\rho_w} \int_0^1 \frac{\partial}{\partial t} \left(q \frac{\partial p}{\partial \eta} \right) d\eta - \frac{1}{g\rho_w} \int_0^1 \nabla \cdot \left(\mathbf{u} q \frac{\partial p}{\partial \eta} \right) d\eta, \quad (6)$$

125 where g is the acceleration due to gravity and ρ_w is the density of water, the inclusion of which
 126 mean that $P - E$ is in units of ms^{-1} (or mm/day as will be shown in the figures). Since the
 127 limits of integration on η are independent of space and time this can be rewritten with the
 128 time derivative and divergence operator outside of the integral as:

$$P - E = -\frac{1}{g\rho_w} \frac{\partial}{\partial t} \int_0^1 \left(q \frac{\partial p}{\partial \eta} \right) d\eta - \frac{1}{g\rho_w} \nabla \cdot \int_0^1 \left(\mathbf{u}q \frac{\partial p}{\partial \eta} \right) d\eta. \quad (7)$$

129 In the case of data provided on pressure levels we revert to a p coordinate for which Eq. 5
 130 becomes:

$$\frac{\partial q}{\partial t} + \nabla \cdot (\mathbf{u}q) + \frac{\partial}{\partial p} (\omega q) = e - c \quad (8)$$

131 The p -coordinate flux form moisture equation can be vertically integrated from the surface
 132 pressure, p_s , to the top of the atmosphere to derive:

$$P - E = -\frac{1}{g\rho_w} \int_0^{p_s} \frac{\partial q}{\partial t} dp - \frac{1}{g\rho_w} \int_0^{p_s} \nabla \cdot (\mathbf{u}q) dp - \frac{1}{g\rho_w} \omega_s q_s, \quad (9)$$

where the subscript s refers to surface quantities. Noting that:

$$\omega_s = \frac{\partial p_s}{\partial t} + \mathbf{u}_s \cdot \nabla p_s, \quad (10)$$

$$\int_0^{p_s} \frac{\partial q}{\partial t} dp = \frac{\partial}{\partial t} \int_0^{p_s} q dp - q_s \frac{\partial p_s}{\partial t}, \quad (11)$$

$$\int_0^{p_s} \nabla \cdot (\mathbf{u}q) dp = \nabla \cdot \int_0^{p_s} \mathbf{u}q dp - q_s \mathbf{u}_s \cdot \nabla p_s, \quad (12)$$

133 we derive:

$$P - E = -\frac{1}{g\rho_w} \frac{\partial}{\partial t} \int_0^{p_s} q dp - \frac{1}{g\rho_w} \nabla \cdot \int_0^{p_s} \mathbf{u}q dp. \quad (13)$$

134 This is the form of the moisture budget equation that we focus most of the analysis on.
 135 However this form only allows understanding of the moisture budget (and its variations) to
 136 advance so far. Note that the divergence operates on the vertically integrated moisture field
 137 and does not allow a breakdown of the moisture convergence into a part due to the mass
 138 convergence and a part due to advection of humidity gradients. Therefore an alternative form
 139 is often presented:

$$P - E = -\frac{1}{g\rho_w} \frac{\partial}{\partial t} \int_0^{p_s} q dp - \frac{1}{g\rho_w} \int_0^{p_s} \nabla \cdot (\mathbf{u}q) dp - \frac{1}{g\rho_w} q_s \mathbf{u}_s \cdot \nabla p_s, \quad (14)$$

140 which allows the divergence to be broken down into parts related to a divergent flow $q\nabla \cdot \mathbf{u}$
 141 and a part related to advection $\mathbf{u} \cdot \nabla q$, viz.

$$P - E = -\frac{1}{g\rho_w} \frac{\partial}{\partial t} \int_0^{p_s} q dp - \frac{1}{g\rho_w} \int_0^{p_s} (q\nabla \cdot \mathbf{u} + \mathbf{u} \cdot \nabla q) dp - \frac{1}{g\rho_w} q_s \mathbf{u}_s \cdot \nabla p_s. \quad (15)$$

142 Here the separation into components of moisture divergence due to divergent flow and
 143 advection is only allowed by bringing the divergence operator inside the vertical integral and,
 144 hence, introduces a boundary term, $q_s \mathbf{u}_s \cdot \nabla p_s$, that also needs to be accounted for (and which
 145 is sometimes discussed (Seager and Vecchi 2010; Seager et al. 2010b) but which is also often
 146 ignored (Seager et al. 2007)).

147 These equations have been written in continuous form but in models will be evaluated using
 148 various numerical methods. For example the model that ERA-I is based upon uses a finite
 149 difference method to evaluate vertical derivatives and a semi-Lagrangian method to determine
 150 advective tendencies (ECMWF 2012). Other models use three dimensional semi-Lagrangian
 151 methods. The humidity tendencies induced by these schemes cannot be reproduced using
 152 archived data that already include the effect of the advection even if the data were archived
 153 at the model time step. A numerical method needs to be chosen to evaluate the terms in
 154 the moisture equation with the additional goal that it is general enough to be applicable to a
 155 variety of reanalyses and/or models.

156 The vertically integrated moisture transport is approximated by:

$$\int_0^{p_s} (\mathbf{u}q) dp \approx \sum_{k=1}^{K_{i,j}} \mathbf{u}_k q_k \Delta p_k \quad (16)$$

157 where the summation is over vertical layers, k , of which there are $K_{i,j}$ with i and j indicating
 158 the longitude and latitude location of grid points. In the original η coordinates $K_{i,j}$ is the
 159 same at all grid points but for archived pressure level data $K_{i,j}$ will depend on longitude and
 160 latitude. The divergence operator on a two-dimensional vector \mathbf{F} is evaluated via:

$$\nabla_f \cdot \mathbf{F} \approx \frac{1}{a \cos \phi_j} \left\{ \frac{1}{\lambda_{i+1,j} - \lambda_{i-1,j}} \left[(\lambda_{i,j} - \lambda_{i-1,j}) \frac{F_{i+1,j}^\lambda - F_{i,j}^\lambda}{\lambda_{i+1,j} - \lambda_{i,j}} + (\lambda_{i+1,j} - \lambda_{i,j}) \frac{F_{i,j}^\lambda - F_{i-1,j}^\lambda}{\lambda_{i,j} - \lambda_{i-1,j}} \right] + \frac{1}{\phi_{i,j+1} - \phi_{i,j-1}} \left[(\phi_{i,j} - \phi_{i,j-1}) \frac{\cos \phi_{j+1} F_{i,j+1}^\phi - \cos \phi_j F_{i,j}^\phi}{\phi_{i,j+1} - \phi_{i,j}} + (\phi_{i,j+1} - \phi_{i,j}) \frac{\cos \phi_j F_{i,j}^\phi - \cos \phi_{j-1} F_{i,j-1}^\phi}{\phi_{i,j} - \phi_{i,j-1}} \right] \right\} \quad (17)$$

161 where F^λ and F^ϕ indicate the components of \mathbf{F} in the longitude and latitude directions and ∇_f
 162 is used to indicate a finite difference approximation to the divergence operator on a longitude-
 163 latitude grid. To evaluate moisture divergence, $\mathbf{F}_{i,j}$ is given by:

$$\mathbf{F}_{i,j} = \sum_{k=1}^{K_{i,j}} \mathbf{u}_{i,j,k} q_{i,j,k} \Delta p_{i,j,k}, \quad (18)$$

164 To evaluate the divergence at grid point (i, j) Eq. 17 computes centered differences at mid-
 165 points to the east and west and north and south and then linearly interpolates these in the
 166 λ and ϕ directions back to the (i, j) point. This therefore allows for the case of uneven grid
 167 spacing (quite common in CMIP5 models in the ϕ direction). In the case of an even grid,
 168 which the ERA-I data is served on, Eq. 17 reduces to the familiar form:

$$\nabla_f \cdot \mathbf{F} \approx \frac{1}{a \cos \phi_j} \left(\frac{F_{i+1,j}^\lambda - F_{i-1,j}^\lambda}{\lambda_{i+1,j} - \lambda_{i-1,j}} + \frac{\cos \phi_{j+1} F_{i,j+1}^\phi - \cos \phi_{j-1} F_{i,j-1}^\phi}{\phi_{i,j+1} - \phi_{i,j-1}} \right) \quad (19)$$

169 The vertical integration goes down to the surface pressure as follows. The pressure thickness
 170 of the lowest layer is equal to the surface pressure minus the pressure at the first reported
 171 pressure level above and, within this layer, the values of \mathbf{u} and q used are the ones of the first
 172 pressure level above the surface pressure value. All of these integration and differentiation ap-
 173 proximations introduce errors. In addition, the time resolution of the diagnostic computation
 174 will also causes errors if it does not conform to the actual time step of the model. For example
 175 a calculation done with 6 hourly data would be expected to be more accurate than one done
 176 with daily data.

177 **4. Evaluation of sources of error in diagnostic moisture**
 178 **budget calculations**

179 Here we assess the relative importance of the approximations introduced into diagnostic
 180 computation of moisture budgets as detailed in the prior section.

181 *a. Patterns of $P - E$ and divergence of ERA-I reported vertically integrated moisture diver-*
 182 *gence*

183 First of all the ERA-I reports within its' data archive what is called the vertically inte-
 184 grated moisture divergence which we label MC after multiplying by -1 to convert to moisture
 185 convergence. ERA-I also reports the vertically integrated moisture flux which we label $VIMF$.
 186 It is assumed that these correspond to:

$$\begin{aligned}
 MC &= -\frac{1}{g\rho_w} \sum_{k=1}^K \nabla \cdot \left(\mathbf{u}q \frac{\partial p}{\partial \eta} \Delta \eta \right)_k \\
 &= -\frac{1}{g\rho_w} \nabla \cdot \sum_{k=1}^K \left(\mathbf{u}q \frac{\partial p}{\partial \eta} \Delta \eta \right)_k \\
 &= -\frac{1}{g\rho_w} \nabla \cdot VIMF
 \end{aligned} \tag{20}$$

187 and that the vertical sum is done on the model η grid, as indicated by use of $\frac{\partial p}{\partial \eta} \Delta \eta$. The
 188 i, j subscripts on K have been dropped for simplicity. Note that since this is evaluated on
 189 the model η grid it does not matter whether the divergence operator is inside or outside
 190 the vertical sum. ECMWF report MC and $VIMF$ as both monthly means of daily means
 191 and also as 6 hourly values with the former equal to the average of the four 6 hourly values
 192 within that day. Using a double overbar to indicate climatological monthly means, Figure
 193 1 shows the climatological monthly means for January and July of $\overline{\overline{MC}}$ and precipitation
 194 minus evaporation, $\overline{\overline{P - E}}$, for the ERA-I reanalysis data set, as well as their difference. Not
 195 surprisingly there is a rather close balance between these two but the difference shows that
 196 this is not a perfect match by any means. In reality vertically integrated moisture divergence
 197 on the model grid should differ from $P - E$ by the change in vertically integrated moisture

198 (Eq. 7). Hence we also show this in Figure 1 where it is evaluated for each month as the ERA-
 199 I reported vertically integrated moisture content for the first day of the next month minus
 200 that for the first of the month itself. The change in moisture storage shows the expected
 201 seasonal cycle (moistening in the summer hemisphere, drying in the winter hemisphere) but
 202 this pattern is quite different from the $\overline{\overline{P - E}} - \overline{\overline{MC}}$ one.

203 Consequently, even though the Reanalysis reports a vertically integrated moisture diver-
 204 gence, this does not balance the sum of model $\overline{\overline{P - E}}$ and change in moisture storage. There
 205 are three possible reasons for this. One is that Eq. 20 is an approximation to the moisture
 206 convergence the model effectively sees. This is because the ECMWF model actually updates
 207 its humidity field by applying a semi-Lagrangian scheme to an advective form of the moisture
 208 equation. As such moisture divergence does not need to be evaluated in the updating of the
 209 model but it might be assumed that, to derive MC as a diagnostic, the moisture divergence
 210 is evaluated in spectral space the same way that mass divergence is computed in the model
 211 to evaluate vertical velocities. Another reason for an imbalance is that the ECMWF model
 212 contains a moisture diffusion along η surfaces (ECMWF 2012) but the q tendencies induced
 213 by this are not saved or known (and also cannot be computed from the humidity field after
 214 the fact). The third reason is that the reported P , E , q and MC fields have been influenced
 215 by the data assimilation scheme such that the moisture budget (Eq. 6) need no longer be in
 216 balance because of so-called 'analysis increments' (Trenberth et al. 2011).

217 *b. Error introduced in evaluation of time mean divergence of vertically integrated moisture*
 218 *flux*

219 The imbalance between $P - E$, moisture storage and MC in ERA-I is not of immediate
 220 concern to us. In climate models these will balance more closely because the moisture budget
 221 is closed due to the absence of analysis increments. Hence our main effort is to assess how
 222 well the divergence of vertically integrated moisture can be evaluated diagnostically using
 223 archived data. That is, how well can the MC itself be approximated from archived \mathbf{u} and q
 224 on pressure levels together with p_s ? As discussed, errors will be introduced in the evaluation
 225 of the divergence, in the evaluation of the vertical integral and by the time resolution of the

226 data, each of which will be treated in turn.

227 1) ERROR FROM EVALUATION OF DIVERGENCE

228 ERA-I reports the vertical integral of moisture flux, $VIMF$, of which MC is the conver-
 229 gence, where presumably the convergence has been evaluated to match the evolution of the
 230 moisture in the model as closely as possible. Hence by applying to $VIMF$ the simple centered
 231 difference divergence operator as in Eq. 17 we determine the error introduced because with
 232 archived data the divergence cannot be evaluated to match the model’s method. That is we
 233 evaluate:

$$-\frac{1}{g\rho_w}\nabla\cdot\overline{\overline{VIMF}} \quad c.f. \quad -\frac{1}{g\rho_w}\nabla_f\cdot\overline{\overline{VIMF}}$$

234 Figure 2 shows the reported vertically integrated moisture flux and the difference between
 235 the convergence of this evaluated diagnostically and the actual convergence of it as reported
 236 by ERA-I. The difference between these is considerably larger than any subsequent errors
 237 introduced through decreases in temporal or vertical resolution. Errors introduced by the
 238 divergence operator approximation are concentrated in regions where the spatial gradients in
 239 the moisture convergence field are large. This is expected as the errors in the ∇_f approximation
 240 will appear like derivatives of the divergence field. For example the Pacific and Atlantic
 241 Intertropical Convergence Zones (ITCZs), where the moisture convergence varies in strength
 242 and sign over small meridional distances, are regions of notable error. Coastal regions, where
 243 the moisture convergence also has strong gradients, and mountainous regions are other areas
 244 where the divergence approximation introduces notable errors.

245 Table 1 shows the climatological area averages of root mean square differences between
 246 monthly means of $-\frac{1}{g\rho_w}\nabla_f\cdot\overline{\overline{VIMF}}$ and both $\overline{\overline{MC}}$ and the convergence of vertically integrated
 247 moisture as computed by us. It can be seen there that the largest error comes from the
 248 comparison of $\overline{\overline{MC}}$ with $-\frac{1}{g\rho_w}\nabla_f\cdot\overline{\overline{VIMF}}$, i.e. purely from the evaluation of divergence. The
 249 other root mean square errors in Table 1 are between quantities in which the divergence is
 250 computed by us as in Eq. 17 (see below) and therefore include only errors due to time or
 251 vertical resolution of that data. These are smaller than the error introduced by the divergence

252 evaluation. This error introduced by the evaluation of divergence is, alas, irreducible. The
 253 issue then becomes the extent to which it impacts any analysis of interest, a matter we address
 254 later.

255 2) ERROR INTRODUCED FROM USING TIME RESOLUTION OF ARCHIVED DATA

256 We begin by considering how the moisture balance is impacted by the fact that the archived
 257 data are not at the model time step but are instead stored at the 6 hourly or, perhaps, daily
 258 timescale. In the case of ERA-I the data are 6 hourly and hence ignore the co-variance of \mathbf{u}
 259 and q at shorter timescales. To do this we show in Figure 3 the quantity:

$$-\frac{1}{g\rho_w}\nabla_f\cdot\sum_{k=1}^K\overline{\mathbf{u}_{6,k}q_{6,k}\Delta p_{6,k}}-\overline{MC}$$

260 where the '6' subscript indicates that this is evaluated using 6-hourly data for \mathbf{u} , q and p . In this
 261 case errors are introduced both by the reduced time resolution of the data and by the vertical
 262 integration being performed by us (on 26 levels) rather than by ECMWF in a way presumably
 263 consistent with the model numerics. Quantitatively, the root mean square differences between
 264 the various diagnostic estimates of climatological MC and the actual ERA-I reported values
 265 are given in Table 2. There it can be seen, by comparison to Table 1, that \overline{MC} is actually
 266 closer to the divergence of our vertically integrated moisture flux than it is to the divergence of
 267 the ERA-I reported vertically integrated moisture flux. This is something we cannot explain
 268 though it implies compensating errors in our computation of divergence and vertical integrals.
 269 Despite this nagging issue, Figure 3 shows that, apart from a hint of systematic error near
 270 the ITCZ, the errors from time resolution and vertical integration appear randomly scattered
 271 around the globe. The ITCZ errors may be due to the existence in that region of transient
 272 storm systems with co-varying winds and humidity on the less than 6 hourly timescale.

273 Figure 3 also shows the quantity:

$$-\frac{1}{g\rho_w}\nabla_f\cdot\sum_{k=1}^K\overline{\mathbf{u}_{d,k}q_{d,k}\Delta p_{d,k}}-\overline{MC}$$

274 where the d subscript indicates this was evaluated with daily data. In this case errors are
 275 systematic with too little moisture divergence at the subtropical edge of the mid-latitudes

276 and too little moisture convergence in the mid-to-high latitudes. This clearly represents an
277 underestimation of poleward moisture transport by mid-latitude transient eddies with the
278 error arising from not sampling the sub-daily co-variance between the flow and the humidity.
279 Since these mid-latitude storms have characteristic timescales of a few to several days it is
280 reasonable that daily resolution data will be inadequate to capture their effects. This point is
281 made clear in Figure 3 where we show the difference between the 6-hourly and daily moisture
282 convergence with the former having stronger subtropical to mid-latitude moisture transport
283 with divergence on the subtropical side and convergence on the poleward side.

284 3) ERROR FROM VERTICAL INTEGRATION USING FEWER PRESSURE LEVELS

285 The calculations so far in which we performed the vertical integration used 26 vertical
286 levels which is more than is common in archives of model data. Hence we redo the integrations
287 with daily data but with a degraded 18 level data set which has fewer model levels near the
288 surface. Figure 4 shows the difference between a 18 layer vertical integration of the moisture
289 convergence and MC_6 , (which can be compared with Figure 3 for the 26 layer case) and
290 the difference between the 26 and 18 layer integrations, all using daily data. As expected,
291 the errors are in general larger when using fewer layers but these are restricted to land while
292 differences over the ocean are small (also see Table 3). The increased error over land is because
293 of less resolution in the lower atmosphere where the moisture is located and also where vertical
294 gradients of moisture are often large.

295 6-hourly data is really required for evaluating the transient contributions to moisture bud-
296 gets but archiving 6-hourly, or even daily, data for complete model runs at model vertical
297 resolution places a considerable stress on data storage requirements and, once archived, on
298 networks used to transfer data from the modeling groups that produce it to researchers else-
299 where that analyze it. In many cases, therefore, the 6-hourly or daily data is archived on a
300 subset of vertical levels to reduce the amount of data archived. For example, examining the
301 current CMIP5 archive of 6-hourly and daily data, it was found that the 6-hourly data was typ-
302 ically only available on 3 vertical levels, obviously inadequate for moisture budget evaluation,
303 and that daily data was available typically on 8 vertical levels. Hence we next determined

304 how closely an evaluation with daily data on 8 levels can match the actual convergence of
 305 vertically integrated moisture, i.e. the comparison:

$$\overline{\overline{MC}} \quad c.f. \quad - \frac{1}{g\rho_w} \nabla_f \cdot \sum_{k=1}^8 \overline{\overline{\mathbf{u}_{d,k} q_{d,k} \Delta p_{d,k}}}$$

306 This comparison already includes the error in going to daily data from time step data (as
 307 in $\overline{\overline{MC}}$) or 6-hourly data and the error in going from 26 levels to 18 levels and then introduces
 308 an additional error in going to 8 levels from 18. However, we choose to show the total error in
 309 Figure 4. Comparing to the 18 level data, the 8 level case introduces significantly more error
 310 across the globe with notable errors appearing in the ITCZ regions and already existing errors
 311 over land becoming much larger. The degradation of the balance in the moisture budget when
 312 reducing the vertical resolution to only 8 levels is really quite striking.

313 4) ERROR INTRODUCED BY IGNORING THE SUB-MONTHLY VARIATIONS OF SURFACE
 314 PRESSURE

315 Up to now the vertical integrals have been performed at the temporal resolution of the
 316 data (e.g. each 6 hours or day) using the surface pressure at the same temporal resolution
 317 as the lower limit of integration. This allows for any co-variation between flow fields, specific
 318 humidity and surface pressure. However it is our experience that high temporal resolution
 319 surface pressure data is not always available so next we address the error introduced by first
 320 computing the time mean of the covariance of \mathbf{u} and q and then vertically integrating this
 321 using the time mean surface pressure. Introducing a single overbar to denote a monthly mean,
 322 we perform the comparisons:

$$\begin{aligned} -\frac{1}{g\rho_w} \nabla_f \cdot \sum_{k=1}^K \overline{\overline{\mathbf{u}_{6,k} q_{6,k} \Delta p_{6,k}}} \quad c.f. \quad & -\frac{1}{g\rho_w} \nabla_f \cdot \sum_{k=1}^K \overline{\overline{\mathbf{u}_{6,k} q_{6,k} \Delta p_{6,k}}} \\ -\frac{1}{g\rho_w} \nabla_f \cdot \sum_{k=1}^K \overline{\overline{\mathbf{u}_{d,k} q_{d,k} \Delta p_{d,k}}} \quad c.f. \quad & -\frac{1}{g\rho_w} \nabla_f \cdot \sum_{k=1}^K \overline{\overline{\mathbf{u}_{d,k} q_{d,k} \Delta p_{d,k}}} \end{aligned}$$

323 Figure 5 shows this comparison with daily data for both the 18 and 26 layer versions and
 324 with 6-hourly data for 26 layers. In no case are there important increases in error when going

325 from daily vertical integrals to calculations that use monthly mean flow-humidity covariances
 326 together with monthly mean pressure thicknesses (see also Table 2). These comparisons show
 327 that no significant additional error is introduced by first time averaging the covariance of \mathbf{u} and
 328 q and then vertically integrating this using the time mean p_s as the lower limit of integration.

329 5. Breaking down the moisture budget into components 330 related to divergent flow, mean flow advection of mois- 331 ture and transient eddy fluxes

332 The form of the moisture budget equation examined so far is quite useful and would allow
 333 a break down of, say, $P - E$ anomalies (or change) into components due to circulation and
 334 humidity anomalies (or change) since either \mathbf{u} or q can be held at climatological values while
 335 the other one is allowed to vary, all within the vertical integral and the divergence operator
 336 (see below). However this form does not allow an assessment of the relative roles of divergent
 337 circulations (i.e. the $q\nabla \cdot \mathbf{u}$ term) and advection of moisture (i.e. the $\mathbf{u} \cdot \nabla q$ term) to $P - E$. In
 338 order to assess that we must return to a form with the divergence operator inside the vertical
 339 integral which then introduces the surface boundary term as in Eqs. 14 and 15. The problem
 340 then emerges when trying to evaluate the $\int_0^{p_s} \nabla \cdot (\mathbf{u}q) dp$ term because, in the presence of varying
 341 surface pressure, the lower limit of integration is different at the grid points used to perform
 342 the divergence operator. For example is the right approach to evaluate $\nabla \cdot (\mathbf{u}q) \approx \nabla_f \cdot (\mathbf{u}q)$
 343 only at the pressure levels that exist for all the points used in the divergence operator (Eq.
 344 15), $(i + 1, j)$, $(i - 1, j)$, $(i, j + 1)$, $(i, j - 1)$, or is the right approach to also incorporate grid
 345 points that are at pressure levels which are nonexistent (higher pressure than surface pressure)
 346 and assume that \mathbf{u} is zero at those points? And, in either case, how is the surface boundary
 347 term to be evaluated?

348 Fortunately there is a way to do this that yields the correct answer. To illustrate the
 349 approach we will reduce the problem to (x, p) dimensions and examine:

$$\frac{\partial}{\partial x} \left(\int_0^{p_s} (uq) dp \right) = \int_0^{p_s} \frac{\partial(uq)}{\partial x} dp + u_s q_s \frac{\partial p_s}{\partial x} \quad (21)$$

350 where $x = a\lambda \cos \phi$ and require that the numerical methods chosen to evaluate these terms
 351 ensure a balance.

352 Referring to Figure 6, and temporarily reintroducing i subscripts on K , we use K_i to
 353 indicate the lowest pressure level at grid point i that is above the surface, i.e. has a pressure,
 354 p_{K_i} lower than the surface pressure at the grid point, p_{s_i} . Then Eq. 21, evaluated between
 355 grid points i and $i + 1$, is approximated by:

$$\left[\frac{\partial}{\partial x} \left(\int_0^{p_s} (uq) dp \right) \right]_{i+1/2} \approx \frac{1}{x_{i+1} - x_i} \left\{ \sum_{k=1}^{K_{i+1}} (uq)_{i+1,k} \Delta p_k + (uq)_{i+1, K_{i+1}} (p_{s, i+1} - p_{K+1/2}) - \left[\sum_{k=1}^{K_i} (uq)_{i,k} \Delta p_k + (uq)_{i, K_i} (p_{s, i} - p_{K+1/2}) \right] \right\}. \quad (22)$$

356 Here, for example, at a latitude ϕ , $x_i = a \cos \phi \lambda_i$. Next we let the level $k = kk$ equal the lowest
 357 level with pressure $p = p_{kk}$ for which all the adjacent grid points have $p_s \geq p_{kk}$. Then Eq. 22
 358 can be rewritten as:

$$\left[\frac{\partial}{\partial x} \left(\int_0^{p_s} (uq) dp \right) \right]_{i+1/2} \approx \frac{1}{x_{i+1} - x_i} \left\{ \sum_{k=1}^{kk} [(uq)_{i+1,k} - (uq)_{i,k}] \Delta p_k + \sum_{k=kk+1}^{K_{i+1}} (uq)_{i+1,k} \Delta p_k - \sum_{k=kk+1}^{K_i} (uq)_{i,k} \Delta p_k + (uq)_{i+1, K_{i+1}} (p_{s, i+1} - p_{K+1/2}) - (uq)_{i, K_i} (p_{s, i} - p_{K+1/2}) \right\} \quad (23)$$

359 where it is understood that the sum $\sum_{k=kk+1}^K$ is only performed for $K \geq kk + 1$ which, by
 360 definition, means only at $i + 1$ for surface height decreasing westward and i for surface height
 361 increasing westward.

362 The first right hand side term in Eq. 23 provides a straightforward approximation to the
 363 first right hand side term in Eq. 21 viz:

$$\left[\int_0^{p_s} \frac{\partial(uq)}{\partial x} dp \right]_{i+1/2} \approx \sum_{k=1}^{kk} \frac{(uq)_{i+1,k} - (uq)_{i,k}}{x_{i+1} - x_i} \Delta p_k \quad (24)$$

364 The remainder of Eq. 22 provides an approximation to the surface term in Eq. 20 as follows:

$$\left(u_s q_s \frac{\partial p_s}{\partial x} \right)_{i+1/2} = \frac{1}{x_{i+1} - x_i} \left\{ \sum_{k=k+1}^{K_{i+1}} (uq)_{i+1,k} \Delta p_k - \sum_{k=k+1}^{K_i} (uq)_{i,k} \Delta p_k + (uq)_{i+1,K_{i+1}} (p_{s,i+1} - p_{K+1/2}) - (uq)_{i,K_i} (p_{s,i} - p_{K+1/2}) \right\} \quad (25)$$

365 We refer to this surface term as SFC_K . The fact that this approximation holds can be seen
 366 by supposing the special case when uq is uniform everywhere and hence equals $(u_s q_s)_{i+1/2}$ in
 367 which case Eq. 25 reduces to:

$$\left(u_s q_s \frac{\partial p_s}{\partial x} \right)_{i+1/2} = (u_s q_s)_{i+1/2} \frac{p_{s,i+1} - p_{s,i}}{x_{i+1} - x_i} \quad (26)$$

368 If the surface term is evaluated as in Eq. 25 and the vertical integral of the divergence of
 369 moisture as in Eq. 24 then the sum of these two terms will exactly equal that given by Eq.
 370 22 (or 23) and the balance in Eq. 21 is assured. As such, since typically all data needed to
 371 evaluate both Eq. 22 and 24 are typically available, we would recommend that the surface
 372 term be evaluated as the difference between these and avoid the need to explicitly calculate it
 373 from Eq. 25.

374 It should be noted that the surface term, despite not being easily interpreted in a physical
 375 way, is not small. In Figure 7 we show the annual mean climatological moisture budget terms
 376 for the vertical integral of moisture divergence (the two dimensional analog of Eq. 24) and the
 377 surface term (the two dimensional analog of Eq. 25, but evaluated as a residual between two
 378 dimensional analogs of Eqs. 23 (or 22) and 24). It is clear that, for the moisture transport by
 379 the mean flow, the pattern and amplitude is preserved whether the convergence is computed
 380 before or after the vertical integral is performed. However it is also clear that the surface term,
 381 $\overline{\overline{SFC}_K}$, is large wherever there are large gradients of surface pressure such as at coasts (where
 382 altitude can change abruptly) and over mountain ranges and, hence, cannot be ignored in the
 383 moisture budget.

384 Bringing the divergence operator inside the vertical integral allows the moisture diver-
 385 gence term to be broken into components related to the divergent flow and to advection across
 386 humidity gradients as in Eq. 15. This is usually performed in the monthly mean fields. Denot-
 387 ing ERA-reported monthly means by a single overbar, in Figure 7 we also show climatological

388 values of the terms in:

$$-\frac{1}{g\rho_w} \sum_{k=1}^{kk} \overline{\nabla_f \cdot (\bar{\mathbf{u}}_k \bar{q}_k \bar{\Delta p}_k)} = -\frac{1}{g\rho_w} \sum_{k=1}^{kk} \overline{(\bar{q}_k \nabla_f \cdot \bar{\mathbf{u}}_k) \bar{\Delta p}_k} - \frac{1}{g\rho_w} \sum_{k=1}^{kk} \overline{(\bar{\mathbf{u}} \cdot \nabla_f \bar{q}_k) \bar{\Delta p}_k} \quad (27)$$

389 Comparison of the mean flow moisture convergence (left side of Eq. 27, top right) with
 390 the total moisture convergence (top left) shows how dominant the mean flow is in explaining
 391 the moisture budget while the differences show the importance of the transient eddies in the
 392 mid-latitudes and subtropics. The mass divergence is clearly the dominant term in explaining
 393 the pattern of the mean flow moisture divergence. However, the mean flow advection term acts
 394 to dry the tropics, where the trades flow from drier regions to moister regions, and moistens
 395 the mid-latitudes. where the surface westerlies flow from moister regions to drier regions.

396 *a. Summary*

397 Table 2 provides a quantitative assessment of the sizes of the various sources of error.
 398 First of all we see that errors are much larger over land than ocean, presumably due to
 399 the complexity of three dimensional spatial structures of winds and humidity. Errors are
 400 also larger in the tropics than extra tropics but this follows from the moisture convergences
 401 and divergences being larger there. The increase in error going from 6 hourly to daily data
 402 is, however, concentrated in the extra tropics and is related to the transient eddy moisture
 403 transport as shown in Figure 3. Errors due to reduced vertical resolution are not striking in
 404 going from 26 to 18 levels but are large over land and ocean, in the tropics and extra tropics,
 405 when going to only 8 levels (typical of CMIP archives of daily data). Using monthly mean
 406 flow-humidity covariances together with monthly mean pressure thicknesses is in all cases an
 407 acceptable approximation.

408 **6. Errors in the evaluation of moisture budget anoma-**
 409 **lies: Case study of the 1993 Mississippi Valley flood**

410 We have demonstrated the errors that are introduced into moisture budgets when evalu-
 411 ated diagnostically with archived data. However, that was done with climatological moisture
 412 budgets. Next we need to assess the errors involved when analyzing the moisture budget
 413 anomalies associated with certain events of interest such as floods and droughts. It is possible,
 414 after all, that the climatological errors are persistent enough in time that they do not appear
 415 within the anomalous budgets. To examine this we choose the case of the late spring-early
 416 summer 1993 Mississippi Valley flood which represents an extreme seasonal anomaly of $P - E$
 417 sustained by anomalous moisture convergence.

418 The analysis was conducted with the 26 level and 6 hourly data but using integration down
 419 to the monthly mean (as opposed to daily) surface pressure since we showed in Section 4 that
 420 this approximation does not introduce important error. The equation we begin with is then:

$$\overline{(P - E)}_{der} = -\frac{1}{g\rho_w} \nabla_f \cdot \sum_{k=1}^K \overline{\mathbf{u}_{6,k} q_{6,k} \Delta p_{6,k}} \quad (28)$$

421 Here, as before, the single overbar denotes monthly mean quantities and $\overline{(P - E)}_{der}$ indicates
 422 the $P - E$ implied by the evaluated moisture convergence (as opposed to that reported by
 423 ERA-I or implied by the actual moisture convergence, \overline{MC}). We are interested in evaluating
 424 this for the average of May, June and July 1993 (MJJ 1993) when the floods occurred and de-
 425 termining the anomalies relative to the climatological situation. With ERA-I we can evaluate
 426 the moisture convergence anomalies for MJJ 1993 directly from the reported values of MC
 427 and then we can also evaluate this from Eq. 28. Therefore, using the second overbar to denote
 428 the long term climatological monthly mean, and a hat above an overbar to denote a departure
 429 of a particular monthly mean from the climatological value, e.g. $\overline{q} = \overline{\overline{q}} + \widehat{\overline{q}}$ we evaluate:

$$\widehat{MC} = \overline{MC} - \overline{\overline{MC}} \quad (29)$$

$$-\frac{1}{g\rho_w} \nabla_f \cdot \sum_{k=1}^K \widehat{\mathbf{u}_{6,k} q_{6,k} \Delta p_{6,k}} = -\frac{1}{g\rho_w} \nabla_f \cdot \sum_{k=1}^K \overline{\mathbf{u}_{6,k} q_{6,k} \Delta p_{6,k}} - \left(-\frac{1}{g\rho_w} \nabla_f \cdot \sum_{k=1}^K \overline{\overline{\mathbf{u}_{6,k} q_{6,k} \Delta p_{6,k}}} \right) \quad (30)$$

430 In Figure 8 we show for MJJ 1993 (i.e. the average of the anomalies for the three months)
 431 the ERA-I reported vertically integrated moisture convergence anomaly, \widehat{MC} , the estimate of
 432 this using 6-hourly archived data on 26 levels (i.e. the left hand side of Eq. 30), for both the
 433 globe and North America, the ERA-I reported $\widehat{P - E}$ and the change of vertically integrated
 434 moisture across the three month period. Globally, there is a close level of agreement between
 435 the actual column integrated moisture convergence anomaly and that diagnostically calculated
 436 with the largest anomalies being moisture convergence over the central and western equatorial
 437 Pacific and divergence to the north and south and within the Pacific ITCZ, consistent with
 438 outgoing long wave radiation anomalies at the time and related to a waning El Niño (e.g.
 439 Trenberth and Guillemot (1996)). Over North America the agreement is also good and shows
 440 a large and focused moisture convergence anomaly over the upper Mississippi Valley and a
 441 moisture divergence anomaly over most of the southern U.S. and the western Atlantic Ocean.
 442 The ERA-I reported $\widehat{P - E}$ anomaly over North America agrees quite well with \widehat{MC} . The
 443 change in moisture storage is small.

444 To assess the level of agreement between the actual and diagnostically computed anomalies,
 445 in Figure 9 we show the differences between ERA-I reported and diagnostically computed
 446 column integrated moisture convergence for MJJ 1993 and, for comparison, the climatological
 447 MJJ. The climatological error in MJJ is similar in character to that in the other seasons
 448 (Figure 1) and is noisy and not systematic over North America. The MJJ 1993 error is
 449 also not systematic and also smaller than the climatological difference. This means that the
 450 anomalous moisture convergence in any one month or season or, presumably, year can indeed
 451 be estimated in a useful way by the diagnostic computation. That this is so allows further
 452 analysis of dynamical and thermodynamical causes of the anomalies of interest.

To determine causes of $P - E$ anomalies we break down the moisture convergence anomaly

into components due to mean circulation anomalies, mean humidity anomalies and transient eddy moisture flux anomalies. To do this we first note that 6-hourly quantities are given, e.g. for q_6 , by:

$$q_6 = \bar{q} + q'_6 = \bar{\bar{q}} + \hat{q} + q'_6, \quad (31)$$

453 where the prime denotes a departure of 6-hourly data from the monthly mean (which itself
454 equals the climatological monthly mean plus the monthly mean anomaly). Substituting expan-
455 sions like Eq. 31 into Eq. 28 we can derive equations for the monthly mean climatology and
456 anomalies in $\overline{(P - E)}_{der}$ or, equivalently, the diagnostically computed moisture convergence,
457 in terms of components of the flow and humidity fields:

$$\overline{\overline{(P - E)}}_{der} \approx -\frac{1}{g\rho_w} \nabla_f \cdot \sum_{k=1}^K \left(\overline{\bar{\mathbf{u}}_k \bar{q}_k} + \overline{u'_{6,k} q'_{6,k}} \right) \overline{\overline{\Delta p_k}} \quad (32)$$

$$\widehat{(P - E)}_{der} \approx -\frac{1}{g\rho_w} \nabla_f \cdot \sum_{k=1}^K \left(\widehat{\bar{\mathbf{u}}_k \bar{q}_k \Delta p_k} + \widehat{u'_{6,k} q'_{6,k} \Delta p_k} \right), \quad (33)$$

$$\approx -\frac{1}{g\rho_w} \nabla_f \cdot \sum_{k=1}^K \left(\overline{\bar{\mathbf{u}}_k \hat{q}_k} + \widehat{\bar{\mathbf{u}}_k \bar{q}_k} + \widehat{u'_{6,k} q'_{6,k}} \right) \overline{\overline{\Delta p_k}}, \quad (34)$$

458 where, to derive the approximation in Eq. 34, products of monthly anomalies and terms
459 involving $\widehat{\Delta p_k}$ have been neglected. (It was found that, in general, ignoring the surface pressure
460 variations which dictate variations in $\widehat{\Delta p_k}$ introduces little additional error. Further, in the
461 case of Eq. 34, which combines terms that are climatological and terms that are monthly
462 anomalies, it would be ambiguous what to use for $\widehat{\Delta p_k}$ and, hence, using climatological values
463 seems expedient¹.) In Eq. 34 the first term on the right hand side is the anomaly in implied
464 $P - E$ due to anomalies in mean specific humidity working with the climatological circulation,
465 the second term is the anomaly due to the anomaly in mean circulation working with the
466 climatological specific humidity and the third term is the anomaly due to anomalies in the
467 moisture convergence by sub-monthly timescale transient eddies.

¹In Seager et al. (2012) (see also Seager and Naik (2012)) anomalies in moisture budgets were examined using compositing over model El Niño and La Niña events and the pressure integrals were chosen to correspond to surface pressure anomalies during these events but the ambiguity introduced by breakdowns into terms combining climatological and anomaly quantities is not avoided.

468 In Figure 10 we show the combined contribution of the mean flow and mean humidity
469 to the moisture convergence anomaly and also the contribution from transient eddy moisture
470 convergence, using now combinations of 18 and 26 levels and 6-hourly and daily data (i.e.
471 the breakdown in Eq. 33). The mean flow and humidity anomalies caused the moisture
472 convergence anomaly in the central U.S. and this is well approximated with only 18 levels. The
473 contribution of mean flow moisture convergence to the floods is consistent with the persistently
474 strong Great Plains Low Level Jet identified by Weaver et al. (2009). The transient eddy
475 moisture convergence anomaly, in contrast, provides a north-south dipole with divergence
476 over the southeastern U.S. and convergence to the north resulting in a shift northward of
477 the total moisture convergence anomaly. The transient eddy moisture convergence anomaly
478 evaluated with 6-hourly data is well approximated with 18 levels. The transient eddy moisture
479 flux convergence pattern is consistent with the argument of Trenberth and Guillemot (1996)
480 (based on flux anomalies but not on convergence) that the storm track anomalies in MJJ
481 1993 transferred moisture from the Gulf of Mexico into the upper Mississippi valley. When the
482 transient eddy moisture convergence and divergence anomalies are evaluated with daily data
483 the patterns are consistent with their 6-hourly counterparts but are notably weaker. As for
484 the climatological case, it is clear that daily data is inadequate for evaluating transient eddy
485 fluxes and divergence and that accuracy requires 6-hourly data.

486 The next step is to determine the relative contribution to the $P - E$ anomaly of changes in
487 the mean flow and changes in the mean humidity, i.e. the breakdown in Eq. 34. In Fig. 11 we
488 show the mean flow moisture convergence anomaly (repeated from Figure 10), together with
489 the anomalous mean moisture flux vectors, and then the part of this that is caused by the flow
490 anomalies combining with the climatological humidity field, and its associated vectors. The
491 similarity of these two sets of fluxes and convergences indicates clearly that the circulation
492 anomaly is the prime contributor to the $P - E$ anomaly while changes in humidity are less
493 important (but not trivial). This result emphasizes the atmospheric dynamical origin of the
494 MJJ 1993 flood in agreement with earlier studies (Mo et al. 1995; Liu et al. 1998). Figure
495 11 also shows the vectors of the transient eddy moisture flux together with their convergence
496 (repeated from Figure 10) which reveal the northwestward flux of moisture by the eddies from
497 the southeast U.S. towards the upper Mississippi Valley.

498 It is also of interest how the mean flow moisture convergence anomaly is contributed to by
 499 the divergent flow (and balancing vertical motion) and by moisture advection as in Eqs. 15
 500 and 27. In this case we rewrite Eq. 33, with the help of Eqs. 14 and 15, and replacing the
 501 pressure thicknesses with climatological values, as:

$$(\overline{P - E})_{der} \approx -\frac{1}{g\rho_w} \sum_{k=1}^K \left(\overline{\bar{q}_k \nabla_f \cdot \bar{\mathbf{u}}_k} + \overline{\bar{\mathbf{u}}_k \cdot \nabla_f \bar{q}_k} \right) \overline{\Delta p_k} - \frac{1}{g\rho_w} \nabla_f \cdot \sum_{k=1}^K \left(\overline{\mathbf{u}'_{6,k} q'_{6,k}} \right) \overline{\Delta p_k} - \overline{SFC}_K.$$
(35)

502 To perform this breakdown the divergence operator has to be brought inside the vertical inte-
 503 gration and hence the surface term, SFC_K , is reintroduced. Figure 12 shows this breakdown
 504 for MJJ 1993. In the left column we once more show the total anomalous convergence (mean
 505 plus transient flows) of vertically integrated moisture at the top (repeated from Figure 10)
 506 and below it the anomalous vertical integral of the total moisture convergence and the surface
 507 term, SFC_K . As for the climatological case (Figure 7), the pattern and amplitude of anoma-
 508 lous moisture convergence is preserved whether or not the convergence is performed before
 509 or after the vertical integral. However, as before, the surface term is non-negligible over the
 510 North American continent because of the presence of sizable surface pressure gradients. In the
 511 right column of Figure 12 we show the total anomalous mean flow moisture convergence once
 512 more and its breakdown into a part due to the divergent mean flow and a part due to mean
 513 flow advection across mean humidity gradients. Both terms are important with a clear role
 514 for the term involving the mean flow convergence and ascending air in the region of highest
 515 $P - E$ anomaly in the Mississippi Valley but with another clear role for the moisture advection
 516 term but further to the east. The advection term here includes the advection of the mean
 517 specific humidity field by the anomalous flow and, referring to Figure 11, the strong southerly
 518 component to the flow anomalies in MJJ 1993 would create a positive $P - E$ tendency in that
 519 way.

520 Finally for the analysis of the MJJ 1993 Mississippi Valley floods, we examine how well the
 521 anomalies would be captured if only 8 levels of daily data were available, as is typical of CMIP
 522 archives of daily data. The 8 layer version quite reasonably captures the 26 level version of the
 523 total moisture convergence (Figure 13). The errors introduced by going from 26 to 8 levels
 524 are quite random spatially but, in general, are of the magnitude of the field itself.

525 In summary, with 6 hourly data and care and attention in the performance of divergence
526 operators and vertical integrators, and their order of computation, the diagnosed moisture
527 budget can be analyzed and broken down to yield important insights into the causes of major
528 hydroclimate anomalies such as the MJJ 1993 Mississippi floods. Nonetheless, in this case of
529 the MJJ 1993 floods, even an analysis of causes based on just 8 levels of daily data might lead
530 to useful, if not definitive, results.

531 7. Conclusions

532 The ability to diagnose moisture budget variations, and their causes, within reanalyses and
533 atmosphere models, using archived data has been evaluated. The work was performed using
534 the ERA-I reanalysis data which reports the actual vertically integrated moisture fluxes and
535 convergences as computed by the model used for the reanalysis. This allows an assessment
536 of errors introduced by diagnostically evaluating these terms from the archived data. The
537 climatological moisture budget is evaluated as well as anomalies during the Mississippi Valley
538 flood of May-June-July 1993. Due to the assimilation procedure the ERA-I does not have
539 a closed moisture budget and precipitation minus evaporation, $P - E$, does not balance the
540 vertically integrated moisture convergence and tendency. However in diagnostic use of data
541 from climate models, where this balance is more closely assured due to lack of data assimilation,
542 the problem is always the evaluation of the vertically integrated moisture convergence. Hence
543 here we focus on the evaluation of that using the ERA-I reanalysis as our test case. Conclusions
544 are as follows:

- 545 • Estimating the ERA-I reported vertically integrated moisture convergence by applying
546 a centered finite difference scheme to the ERA-I reported vertically integrated moisture
547 fluxes introduces significant error which is greater over land than ocean. This is probably
548 strongly influenced by the use of fundamentally different numerical methods to evaluate
549 terms related to convergence of moisture in the ERA-I model compared to those used in
550 the diagnostic evaluation of moisture convergence. Since the results of methods used in
551 the ERA-I cannot be reproduced using diagnostic data, and the effects of moisture
552 diffusion in the ERA-I also cannot, this error is considered irreducible.

- 553 • In mid-latitudes where transient eddies cause significant time-averaged covariances of
554 flow and humidity and, hence, time averaged moisture fluxes and convergence, use of
555 6-hourly data introduces far less error than daily data. The error from using daily data
556 appears as an underestimation of transient eddy moisture fluxes and convergence.

- 557 • Using 18 vertical levels instead of 26 vertical levels, with loss of vertical resolution in
558 the boundary layer, introduces additional errors primarily over land areas and has little
559 effect over the ocean presumably because of differences in the complexity of the vertical
560 structure of winds and humidity. However, going from 18 levels to the 8 levels typi-
561 cal of CMIP archives of daily data, introduces additional errors which are now spread
562 across both land and ocean. Monthly mean data in CMIP archives is usually stored
563 at greater vertical resolution. Calculating the mean flow moisture convergence at the
564 higher resolution and the transient contribution at the reduced vertical resolution will
565 reduce error.

- 566 • Daily surface pressure data is not always available in model archives. However, per-
567 forming vertical integrals with monthly mean pressure fields does not cause a significant
568 increase in error compared to performing vertical integrals each day with daily pressure
569 fields or each 6 hours with 6-hourly pressure fields.

- 570 • When breaking down mean flow moisture convergence into components due to mass flux
571 convergence and advection, the divergence operator has to be taken inside the vertical
572 pressure integral which introduces a surface term, $q_s \mathbf{u}_s \cdot \nabla p_s$. A method is developed
573 to numerically evaluate the vertical integral of mean flow moisture convergence and
574 the surface term that assures that these sum exactly to equal the convergence of the
575 vertically integrated moisture flux.

- 576 • Errors in diagnostically evaluating moisture budgets are no larger, and maybe smaller,
577 for individual seasonal anomalies than for climatologies which allows the causes of hy-
578 droclimate anomalies to be examined.

- 579 • The anomalous moisture budget evaluation was illustrated for the case of the Mississippi
580 floods of May-June-July 1993. The diagnostically computed moisture convergence closely

581 matches the ERA-I reported one as well as the ERA-I $P - E$. It is shown that mean
582 flow moisture convergence related to a southerly flow anomaly and convergent flow was
583 responsible for the positive $P - E$ in the central U.S. while an anomalous transient
584 eddy moisture flux divergence dried the southeast U.S. and transient eddy moisture flux
585 convergence moistened the upper Mississippi valley. It is also shown that the moisture
586 budget anomalies responsible for the flood were largely caused by circulation anomalies
587 combining with the mean flow with the impacts of humidity anomalies being weaker.
588 The contribution of the circulation anomalies was effected through both changes in
589 mass convergence (and hence vertical motion) and changes in the advection of the mean
590 humidity. The transient eddy contribution to the anomaly was underestimated with
591 hourly data. However, an analysis with even 8 levels of daily data would reveal the
592 major causes of the flood.

593 Floods and droughts are the major sources of harm to people and society from weather
594 and climate events and we need to improve our ability to predict them and to plan for them
595 whether they can be predicted ahead of time or not. Prediction requires understanding which
596 requires dissecting historical events to determine what the physical mechanisms responsible
597 were. One important aspect of this is the determination of the combination of mean and
598 transient flow and moisture anomalies that caused anomalies in $P - E$ and, hence, droughts
599 and floods. Such work can indicate, for example, the need to predict variations in storm
600 tracks, stationary waves, fluxes of moisture etc. This requires diagnostic evaluation of model
601 and reanalysis moisture budgets. Alas, even using the actual vertically integrated moisture
602 flux, the diagnostic evaluation of moisture divergence causes significant error. Using daily
603 data instead of 6 hourly data leads to a notable underestimation off mid-latitude transient
604 eddy fluxes and reducing vertical resolution to 8 layers greatly increases error.

605 In this regard we make the following recommendation:

606 **Recommendation:** Climate models and reanalyses should compute covariances at the
607 model time step and then average these into monthly means (e.g. archive monthly means of
608 $\mathbf{u}_{T,k}q_{T,k}$, where T refers to time step values on the model vertical grid) for archiving in, for
609 example, CMIP data and in Reanalysis data.

610 Monthly mean flow-humidity covariances can be vertically integrated with the monthly
611 pressure fields to yield an accurate approximation to the total monthly mean convergence
612 of vertically integrated moisture fluxes. With this saved, the transient contributions can be
613 evaluated by subtracting the monthly mean contributions evaluated from the monthly mean
614 data. Transient contributions estimated in this way will in fact be more accurate than those
615 computed with archived 6-hourly data and even more accurate than those computed with
616 daily data at the modest cost of increasing the size of model data archives. If this was done it
617 would allow researchers to perform the accurate analyses of the mean, variability and change in
618 the atmospheric branch of the hydrological cycle needed to advance knowledge of the Earth's
619 climate system.

620 *Acknowledgments.*

621 This work was supported by NOAA award NA10OAR4310137 (Global Decadal Hydrocli-
622 mate Variability and Change). We would like to thank Yochanan Kushnir for useful discussions
623 and Donna Lee for downloading the ERA-Interim data and the European Centre for Medium
624 Range Weather Forecasts for making the reanalysis data available.

REFERENCES

627 Allen, M. R. and W. J. Ingram, 2002: Constraints on future changes in climate and the
628 hydrologic cycle. *Nature*, **419**, 224–232.

629 Cutter, S. L., C. T. Emrich, J. J. Webb, and D. Morath, 2009: Social Vulnerability to Climate
630 Variability Hazards: A Review of the Literature. Tech. rep., Hazards and Vulnerability
631 Research Institute, University of South Carolina, Columbia, SC, 44pp.

632 Dee, D., et al., 2011: The ERA-Interim Reanalysis; configuration and performance of the data
633 assimilation system. *Quart. J. Roy. Meteor. Soc.*, **137**, 553–597.

634 ECMWF, 2012: IFS Documentation Cy37r2 Operational implementation 18 May 2011. Part
635 III: Dynamics and numerical procedures. Tech. rep., European Centre for Medium Range
636 Weather Forecasts, 29 pp.

637 Harnik, N., R. Seager, N. Naik, M. Cane, and M. Ting, 2010: The role of linear wave refrac-
638 tion in the transient eddy-mean flow response to tropical Pacific SST anomalies. *Quart. J.*
639 *Roy. Meteor. Soc.*, 2132–2146.

640 Held, I. M. and B. J. Soden, 2006: Robust responses of the hydrological cycle to global
641 warming. *J. Climate*, **19**, 5686–5699.

642 Intergovernmental Panel on Climate Change, 2007: *Climate Change: The IPCC Scientific*
643 *Assessment*. Cambridge University Press, Cambridge, England, 365 pp.

644 Konor, C. S. and A. Arakawa, 1997: Design of an atmospheric model based on a generalized
645 vertical coordinate. *Mon. Wea. Rev.*, **125**, 1649–1673.

646 Liu, Y. M., M. Ting, and H. Wang, 1998: Maintenance of circulation anomalies during the
647 1988 drought and 1993 floods over the United States. *J. Atmos. Sci.*, **55**, 2810–2832.

648 Mo, K. C., J. Nogues-Paegle, and J. Paegle, 1995: Physical mechanisms of the 1993 summer
649 floods. *J. Atmos. Sci.*, **52**, 879–895.

650 Nakamura, J., U. Lall, Y. Kushnir, A. W. Robertson, and R. Seager, 2012: Dynamical struc-
651 ture of major spring floods in the U.S. Midwest. *J. Hydromet.*, in press.

652 Seager, R., N. Harnik, W. A. Robinson, Y. Kushnir, M. Ting, H. P. Huang, and J. Velez,
653 2005: Mechanisms of ENSO-forcing of hemispherically symmetric precipitation variability.
654 *Quart. J. Roy. Meteor. Soc.*, **131**, 1501–1527.

655 Seager, R. and N. Naik, 2012: A mechanisms-based approach to detecting recent anthropogenic
656 hydroclimate change. *J. Climate*, **25**, 236–261.

657 Seager, R., N. Naik, M. A. Cane, N. Harnik, M. Ting, and Y. Kushnir, 2010a: Adjustment
658 of the atmospheric circulation to tropical Pacific SST anomalies: Variability of transient
659 eddy propagation in the Pacific-North America sector. *Quart. J. Roy. Meteorol. Soc.*, **136**,
660 277–296.

661 Seager, R., N. Naik, and G. Vecchi, 2010b: Thermodynamic and dynamic mechanisms for
662 large-scale changes in the hydrological cycle in response to global warming. *J. Climate*, **23**,
663 4651–4668.

664 Seager, R., N. Naik, and L. Vogel, 2012: Does global warming cause intensified interannual
665 hydroclimate variability? *J. Climate*, **25**, 3355–3372.

666 Seager, R. and G. A. Vecchi, 2010: Greenhouse warming and the 21st Century hydroclimate
667 of southwestern North America. *Proc. Nat. Acad. Sci.*, **107**, 21 277–21 282.

668 Seager, R., et al., 2007: Model projections of an imminent transition to a more arid climate
669 in southwestern North America. *Science*, **316**, 1181–1184.

670 Trenberth, K., J. T. Fasullo, and J. Mackaro, 2011: Atmospheric moisture transport from
671 ocean to land and global energy flows in Reanalyses. *J. Climate*, **24**, 4907–4924.

672 Trenberth, K. and C. J. Guillemot, 1996: Physical processes involved in the 1988 drought and
673 1993 floods in North America. *J. Climate*, **9**, 1288–1298.

674 Weaver, S. J., A. Ruiz-Barradas, and S. Nigam, 2009: Pentad evolution of the 1988 drought
675 and 1993 flood over the Great Plains: An NARR perspective on the atmospheric and
676 terrestrial water balance. *J. Climate.*, **22**, 5366–5384.

677 TABLE 1. The long term average of root mean square differences (mm/day) between the
678 monthly mean diagnostically computed convergence of ERA-I reported vertically integrated
679 moisture flux ($\nabla_f \cdot VIMF$) and, left column, the ERA-I reported monthly mean vertically
680 integrated moisture convergence (MC) and, right columns, diagnostically computed
681 convergences of diagnostically computed monthly mean vertical moisture fluxes.

$$rms((\cdot) - \nabla_f \cdot VIMF)$$

	MC	6 hourly, 26 levels	6 hourly, 18 levels	6 hourly, 8 levels
Global	1.31	0.93	1.04	1.89
Land	1.94	1.34	1.53	2.82
Ocean	0.95	0.70	0.76	1.35
30°S-30°N	1.21	0.86	0.94	1.71
30°-90°	0.53	0.45	0.47	0.77

682

683 TABLE 2. The long term average of root mean square differences (mm/day) between
684 monthly mean diagnostically computed divergence of vertically integrated moisture content
685 and the ERA-I reported values of the same (\overline{MC}) for various combinations of vertical and
686 time resolution of the diagnostic computations. Legend in the table corresponds to the usage
687 in the main text except that n generically refers to the time resolution, either 6 hourly or
688 daily.

Errors (mm/day)

	26 levels			18 levels			8 levels		
	$\overline{\overline{\mathbf{u}_n q_n \Delta p_n}}$	$\overline{\overline{\mathbf{u}_n q_n \Delta p}}$	$\overline{\overline{\mathbf{u}_n q_n \Delta p}}$	$\overline{\overline{\mathbf{u}_n q_n \Delta p_n}}$	$\overline{\overline{\mathbf{u}_n q_n \Delta p}}$	$\overline{\overline{\mathbf{u}_n q_n \Delta p}}$	$\overline{\overline{\mathbf{u}_n q_n \Delta p_n}}$	$\overline{\overline{\mathbf{u}_n q_n \Delta p}}$	$\overline{\overline{\mathbf{u}_n q_n \Delta p}}$
6 hour									
Global	1.10	1.11	1.11	1.20	1.21	1.22	1.97	2.02	2.07
Land	1.57	1.57	1.57	1.74	1.76	1.79	2.90	3.00	3.08
Ocean	0.85	0.85	0.85	0.89	0.90	0.90	1.43	1.46	1.49
$\leq 30^\circ$	1.06	1.06	1.06	1.12	1.12	1.12	1.81	1.83	1.86
30°-90°	0.52	0.52	0.52	0.54	0.55	0.56	0.82	0.86	0.91
daily									
Global	1.14	1.14	1.14	1.23	1.24	1.26	1.99	2.04	2.09
Land	1.58	1.59	1.59	1.76	1.78	1.80	2.91	2.99	3.07
Ocean	0.89	0.89	0.90	0.94	0.94	0.95	1.47	1.49	1.52
$\leq 30^\circ$	1.07	1.07	1.07	1.13	1.13	1.13	1.82	1.84	1.86
30°-90°	0.64	0.64	0.64	0.66	0.67	0.68	0.93	0.97	1.01

690 List of Figures

- 691 1 The January (left column) and July (right column) climatologies of the ERA-
692 Interim reported 'vertically-integrated moisture divergence', $\overline{\overline{MC}}$ (top), $\overline{\overline{P - E}}$
693 (upper middle), their difference (lower middle) and the change in moisture stor-
694 age computed from the reported vertically integrated moisture content (bot-
695 tom). Units are mm/day 36
- 696 2 The January (left column) and July (right column) climatologies of the ERA-
697 Interim reported 'vertically-integrated moisture flux', $\overline{\overline{VIMF}}$ (top) and the dif-
698 ference between the divergence of this as evaluated using a centered finite differ-
699 ence scheme and the ERA-Interim reported value $\overline{\overline{\nabla_f \cdot VIMF}} - \overline{\overline{MC}}$ (bottom).
700 Units are mm/day 37
- 701 3 The January (left column) and July (right column) climatological differences
702 between the ERA-I reported vertically-integrated moisture convergence $\overline{\overline{MC}}$
703 (top) and that evaluated using archived 6-hourly data on 26 pressure levels
704 (top), daily data on 26 pressure levels (middle) and the difference between 6-
705 hourly and daily evaluations (bottom). Units are mm/day 38
- 706 4 The January (left column) and July (right column) climatological differences
707 between the ERA-I reported vertically-integrated moisture convergence $\overline{\overline{MC}}$
708 (top) and that evaluated using archived daily data on 18 pressure levels (top),
709 8 pressure levels (middle) and the difference between evaluations using daily
710 data and 26 levels versus 18 levels (bottom). Units are mm/day 39

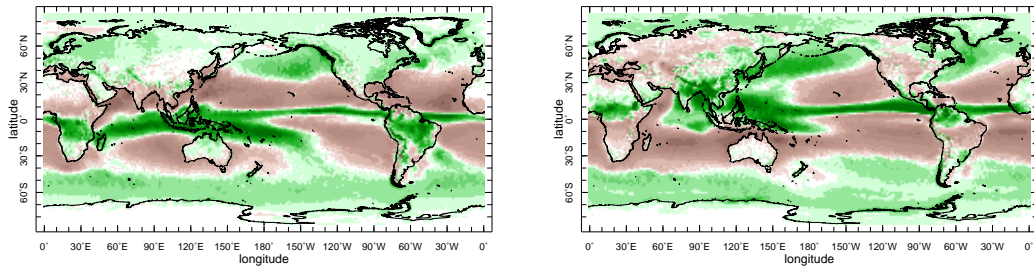
- 711 5 The January (left column) and July (right column) climatological differences
712 between evaluations of the convergence of vertically integrated moisture for the
713 cases of using monthly means of daily wind and humidity covariances combined
714 with monthly mean pressure thicknesses and the case that allows for daily
715 covariances of wind, humidity and pressure thicknesses with 18 pressure levels
716 (top), 26 pressure levels (bottom) and the same difference using 26 pressure
717 levels (bottom). Units are mm/day 40
- 718 6 Schematic of a pressure grid over uneven topography for reference in discussion
719 of how to evaluate the surface term that appears when evaluating vertical in-
720 tegrals of moisture divergence, i.e. when the divergence operator is inside the
721 vertical integral over pressure. K_i and K_{i+1} indicate number of vertical pres-
722 sure levels at columns i and $i + 1$, k_k indicates the lowest level for which the
723 the pressure, p_k is lower than the surface pressure at both grid points, i and
724 $i + 1$, needed to evaluate the divergence operator at $i + 1/2$. 41
- 725 7 The annual mean climatology of the convergence of vertically integrated total
726 moisture flux (top left) and its two components, the vertical integral of total
727 moisture convergence (middle left) and the total surface term (bottom left).
728 The convergence of vertically integrated mean flow moisture flux (top right)
729 is split into components due to the convergence mean flow (middle right) and
730 mean flow advection (bottom right). Units are mm/day 42
- 731 8 The ERA-Interim reported (top and middle left) vertically integrated moisture
732 convergence anomaly, and that computed diagnostically from 6 hourly data on
733 26 levels (top and middle right) for May-June-July 1993 for the planet (top)
734 and North America (middle). At lower left the ERA-I reported $\widehat{P - E}$ is shown
735 and at bottom right the change in moisture storage. Units are mm/day 43

736	9	The difference between ERA-I reported vertically integrated moisture convergence and that computed diagnostically with 6 hourly data on 26 levels for climatological MJJ and just for MJJ 1993 (right) . Units are mm/day	44
737			
738			
739	10	Components of the MJJ 1993 moisture budget anomaly. The contribution from anomalies in the mean flow and mean humidity evaluated with 26 levels (top left) and 18 levels (top right), the contribution from transient eddy moisture flux convergence evaluated with 6 hourly data (middle) and daily data (bottom) and for 26 levels (left) and 18 levels (right). Units are mm/day	45
740			
741			
742			
743			
744	11	The MJJ 1993 mean flow moisture flux anomaly and its convergence evaluated with 26 levels (top) and the part of this due to just mean flow anomalies combining with climatological humidity together with its convergence (middle) and the transient eddy moisture fluxes and their convergence evaluated with climatological pressure thicknesses (bottom). Units are <i>kg/m/s</i> for the fluxes and <i>mm/day</i> for the convergence.	46
745			
746			
747			
748			
749			
750	12	The MJJ 1993 anomaly of the total convergence of the vertically integrated moisture flux (top left) and its breakdown into the vertical integral of moisture convergence (middle left) and the surface term (bottom left) all using 6 hourly data and 26 levels. The right column shows terms related to the mean flow and mean humidity anomalies. The anomaly of the convergence of vertically integrated mean flow moisture flux (top right), and the components of the vertically integrated moisture convergence due to the mean flow convergence (middle right) and mean flow advection of mean humidity (bottom right). All terms were evaluated using climatological pressure thicknesses. Units are <i>kg/m/s</i> for the fluxes and <i>mm/day</i> for the convergence.	47
751			
752			
753			
754			
755			
756			
757			
758			
759			
760	13	The MJJ 1993 anomaly of the convergence of the total vertically integrated moisture flux computed with 26 layers (top) and 8 layers (middle) and their difference (bottom). Units are <i>mm/day</i> .	48
761			
762			

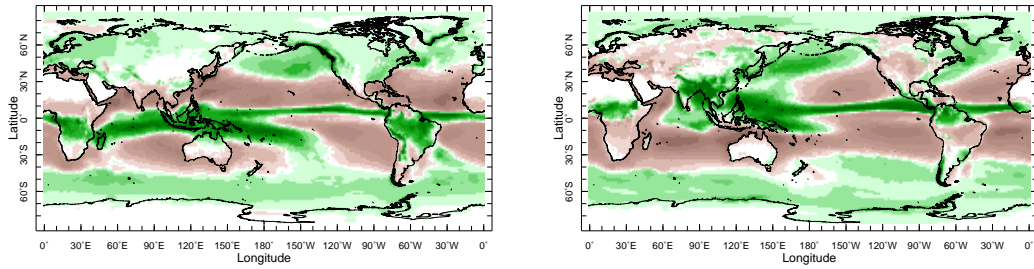
January climatology

July climatology

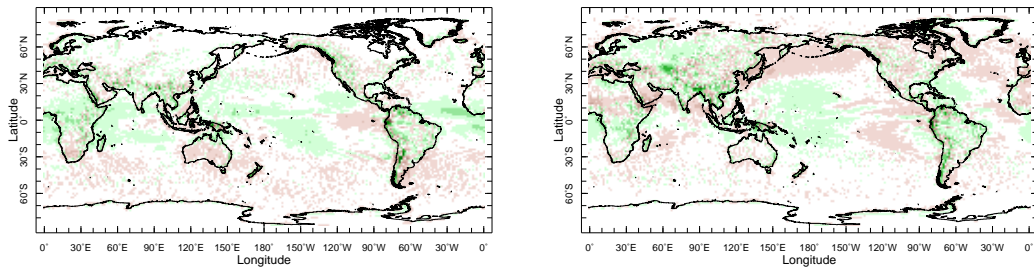
Moisture Convergence, $\overline{\overline{MC}}$



$\overline{\overline{P - E}}$



$\overline{\overline{P - E}} - \overline{\overline{MC}}$



Change in Vertically Integrated Moisture Content

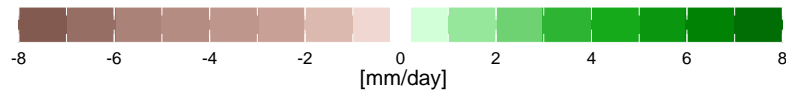
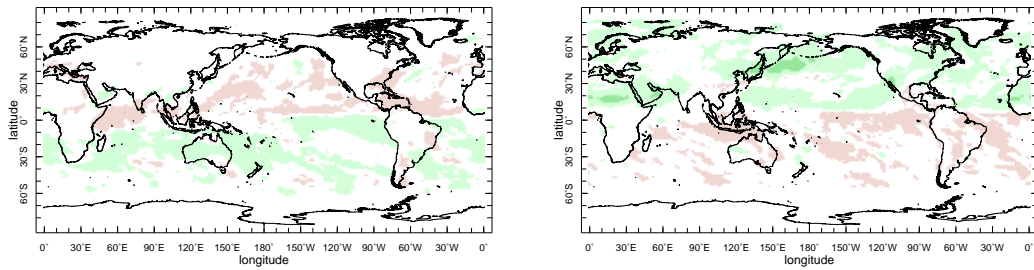
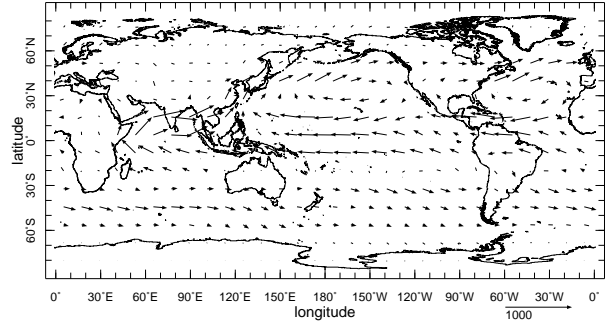
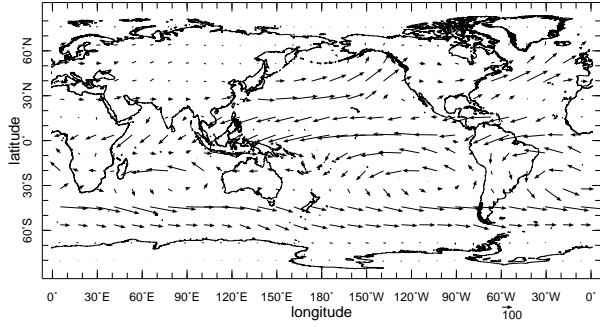


FIG. 1. The January (left column) and July (right column) climatologies of the ERA-Interim reported 'vertically-integrated moisture divergence', $\overline{\overline{MC}}$ (top), $\overline{\overline{P - E}}$ (upper middle), their difference (lower middle) and the change in moisture storage computed from the reported vertically integrated moisture content (bottom). Units are mm/day

January climatology

July climatology

vertically integrated moisture flux, $\overline{\overline{VIMF}}$



$$\overline{\overline{-\frac{1}{g\rho_w}\nabla_f \cdot VIMF}} - \overline{\overline{MC}}$$

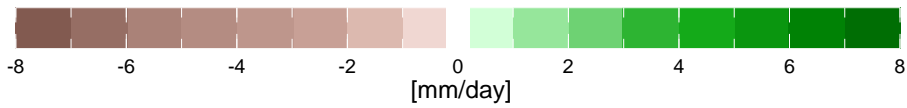
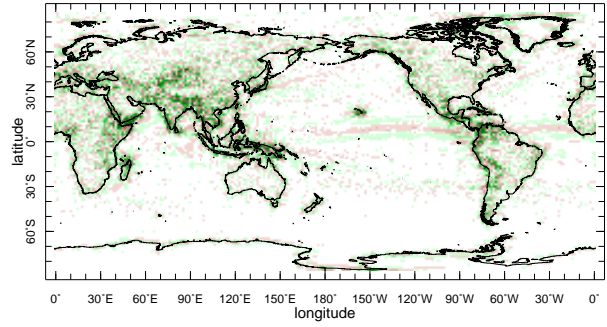
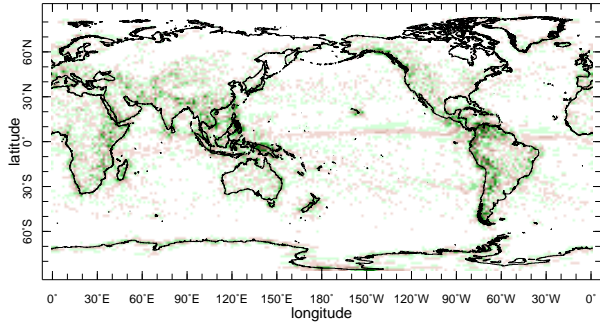
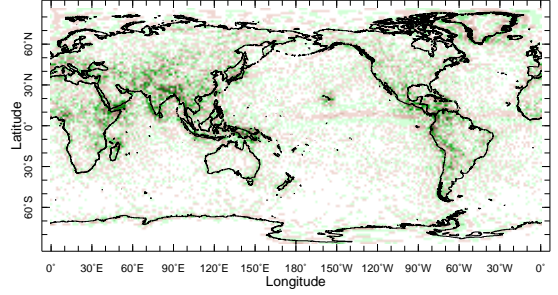
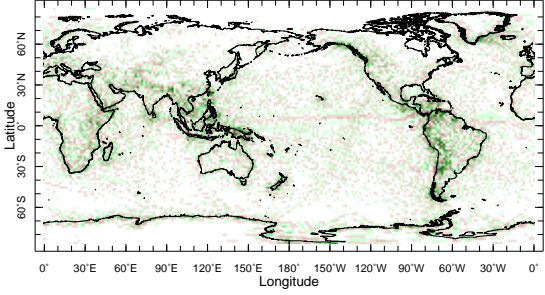


FIG. 2. The January (left column) and July (right column) climatologies of the ERA-Interim reported 'vertically-integrated moisture flux', $\overline{\overline{VIMF}}$ (top) and the difference between the divergence of this as evaluated using a centered finite difference scheme and the ERA-Interim reported value $\overline{\overline{-\nabla_f \cdot VIMF}} - \overline{\overline{MC}}$ (bottom). Units are mm/day

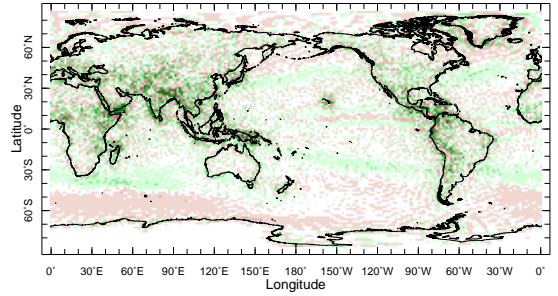
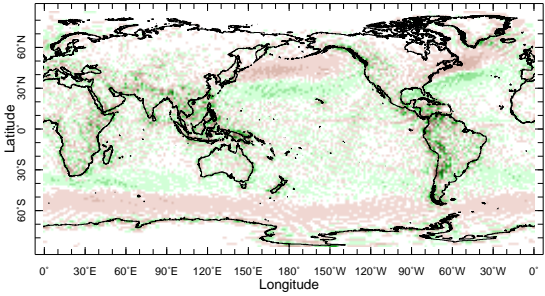
January climatology

July climatology

$$\left(-\frac{1}{g\rho_w}\nabla_f\cdot\sum_{k=1}^{26}\overline{\mathbf{u}_{6,k}q_{6,k}\Delta p_{6,k}}\right)-\overline{MC}$$



$$\left(-\frac{1}{g\rho_w}\nabla_f\cdot\sum_{k=1}^{26}\overline{\mathbf{u}_{d,k}q_{d,k}\Delta p_{d,k}}\right)-\overline{MC}$$



$$\left(-\frac{1}{g\rho_w}\nabla_f\cdot\sum_{k=1}^{26}\overline{\mathbf{u}_{6,k}q_{6,k}\Delta p_{6,k}}\right)-\left(-\frac{1}{g\rho_w}\nabla_f\cdot\sum_{k=1}^{26}\overline{\mathbf{u}_{d,k}q_{d,k}\Delta p_{d,k}}\right)$$

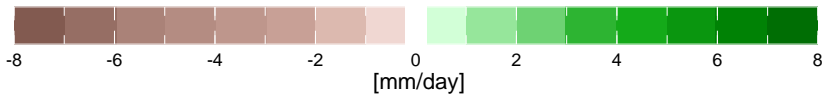
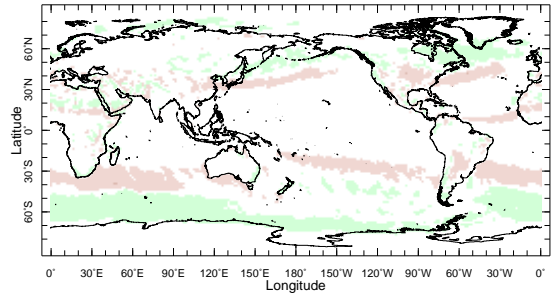
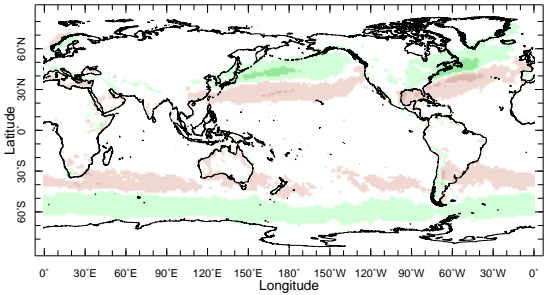
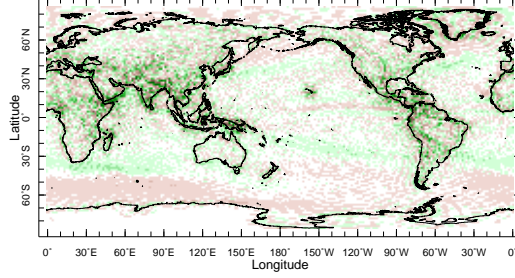
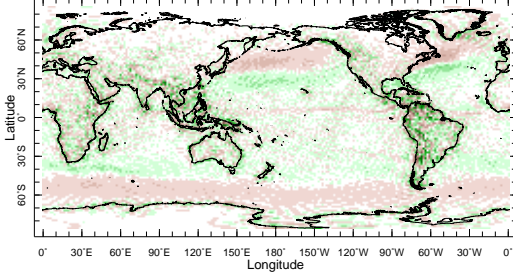


FIG. 3. The January (left column) and July (right column) climatological differences between the ERA-I reported vertically-integrated moisture convergence \overline{MC} (top) and that evaluated using archived 6-hourly data on 26 pressure levels (top), daily data on 26 pressure levels (middle) and the difference between 6-hourly and daily evaluations (bottom). Units are mm/day

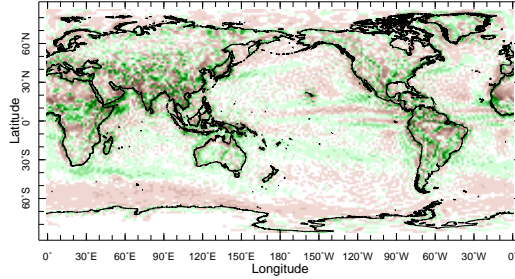
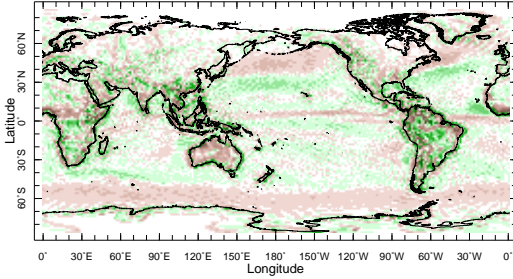
January climatology

July climatology

$$\left(-\frac{1}{g\rho_w}\nabla_f\cdot\sum_{k=1}^{18}\overline{\mathbf{u}_{d,k}q_{d,k}\Delta p_{d,k}}\right)-\overline{MC}$$



$$\left(-\frac{1}{g\rho_w}\nabla_f\cdot\sum_{k=1}^8\overline{\mathbf{u}_{d,k}q_{d,k}\Delta p_{d,k}}\right)-\overline{MC}$$



$$\left(-\frac{1}{g\rho_w}\nabla_f\cdot\sum_{k=1}^{26}\overline{\mathbf{u}_{d,k}q_{d,k}\Delta p_{d,k}}\right)-\left(-\frac{1}{g\rho_w}\nabla_f\cdot\sum_{k=1}^{18}\overline{\mathbf{u}_{d,k}q_{d,k}\Delta p_{d,k}}\right)$$

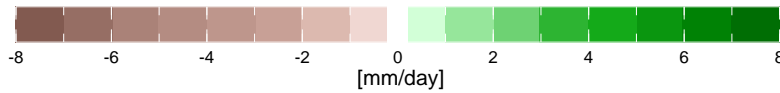
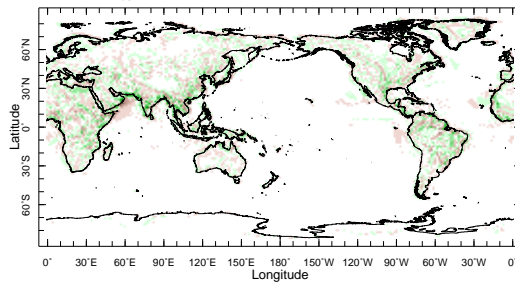
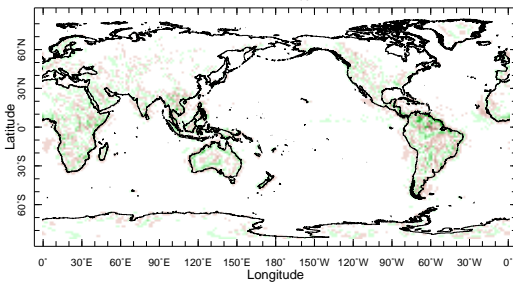


FIG. 4. The January (left column) and July (right column) climatological differences between the ERA-I reported vertically-integrated moisture convergence \overline{MC} (top) and that evaluated using archived daily data on 18 pressure levels (top), 8 pressure levels (middle) and the difference between evaluations using daily data and 26 levels versus 18 levels (bottom). Units are mm/day

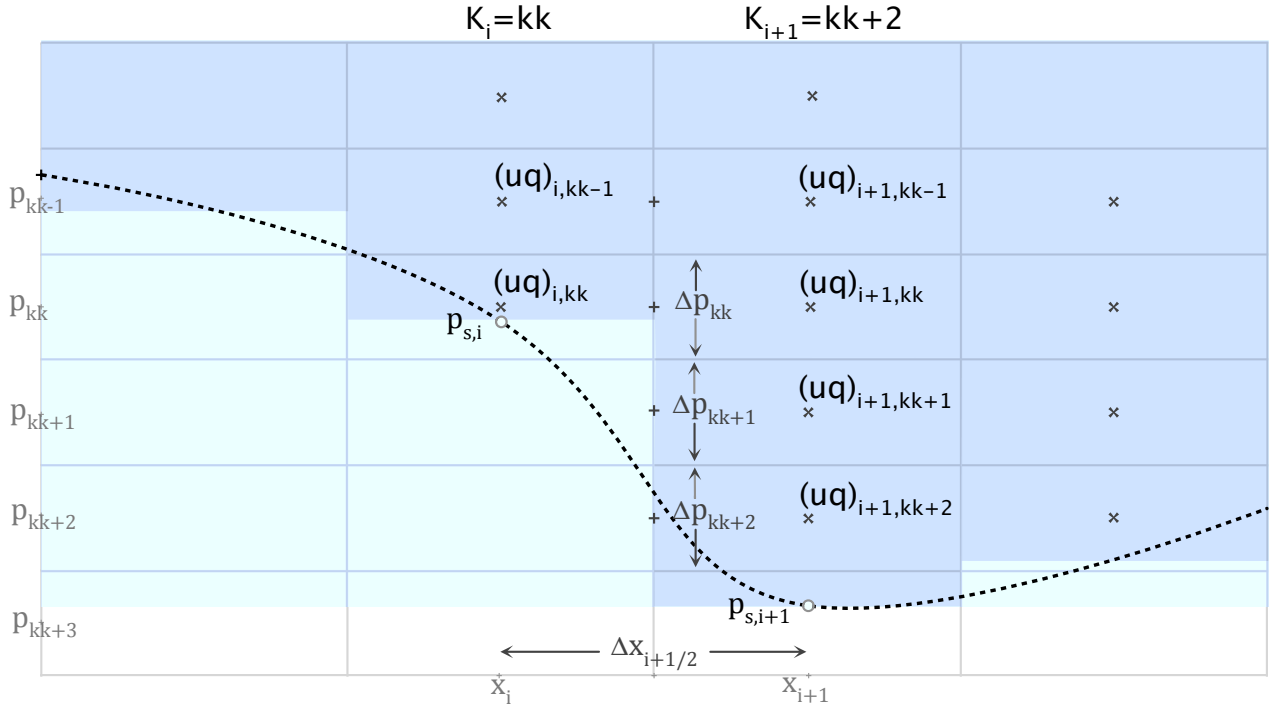


FIG. 6. Schematic of a pressure grid over uneven topography for reference in discussion of how to evaluate the surface term that appears when evaluating vertical integrals of moisture divergence, i.e. when the divergence operator is inside the vertical integral over pressure. K_i and K_{i+1} indicate number of vertical pressure levels at columns i and $i+1$, kk indicates the lowest level for which the pressure, p_k is lower than the surface pressure at both grid points, i and $i+1$, needed to evaluate the divergence operator at $i+1/2$.

Annual Climatology

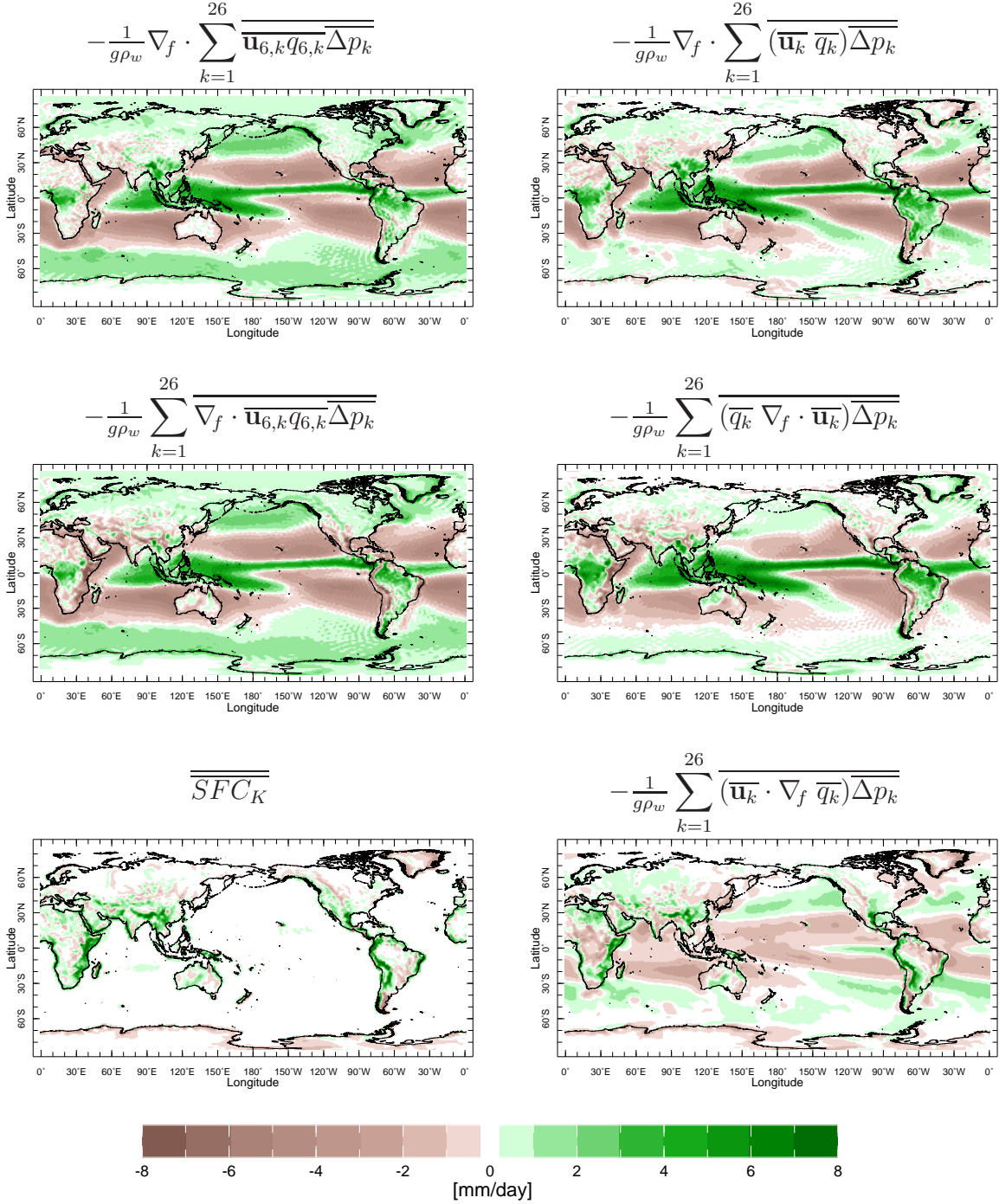


FIG. 7. The annual mean climatology of the convergence of vertically integrated total moisture flux (top left) and its two components, the vertical integral of total moisture convergence (middle left) and the total surface term (bottom left). The convergence of vertically integrated mean flow moisture flux (top right) is split into components due to the convergence mean flow (middle right) and mean flow advection (bottom right). Units are mm/day

MJJ 1993

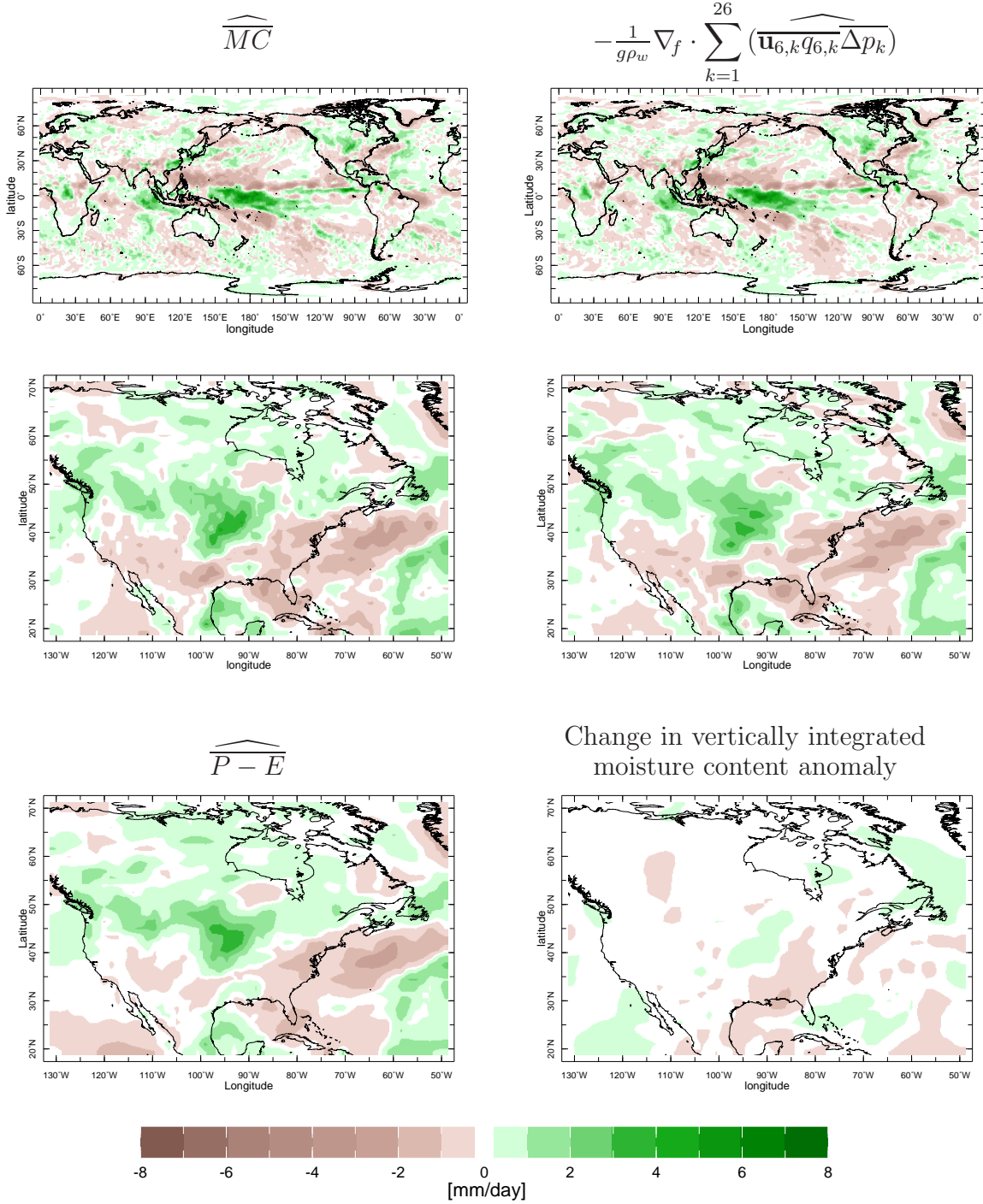


FIG. 8. The ERA-Interim reported (top and middle left) vertically integrated moisture convergence anomaly, and that computed diagnostically from 6 hourly data on 26 levels (top and middle right) for May-June-July 1993 for the planet (top) and North America (middle). At lower left the ERA-I reported $\widehat{P - E}$ is shown and at bottom right the change in moisture storage. Units are mm/day

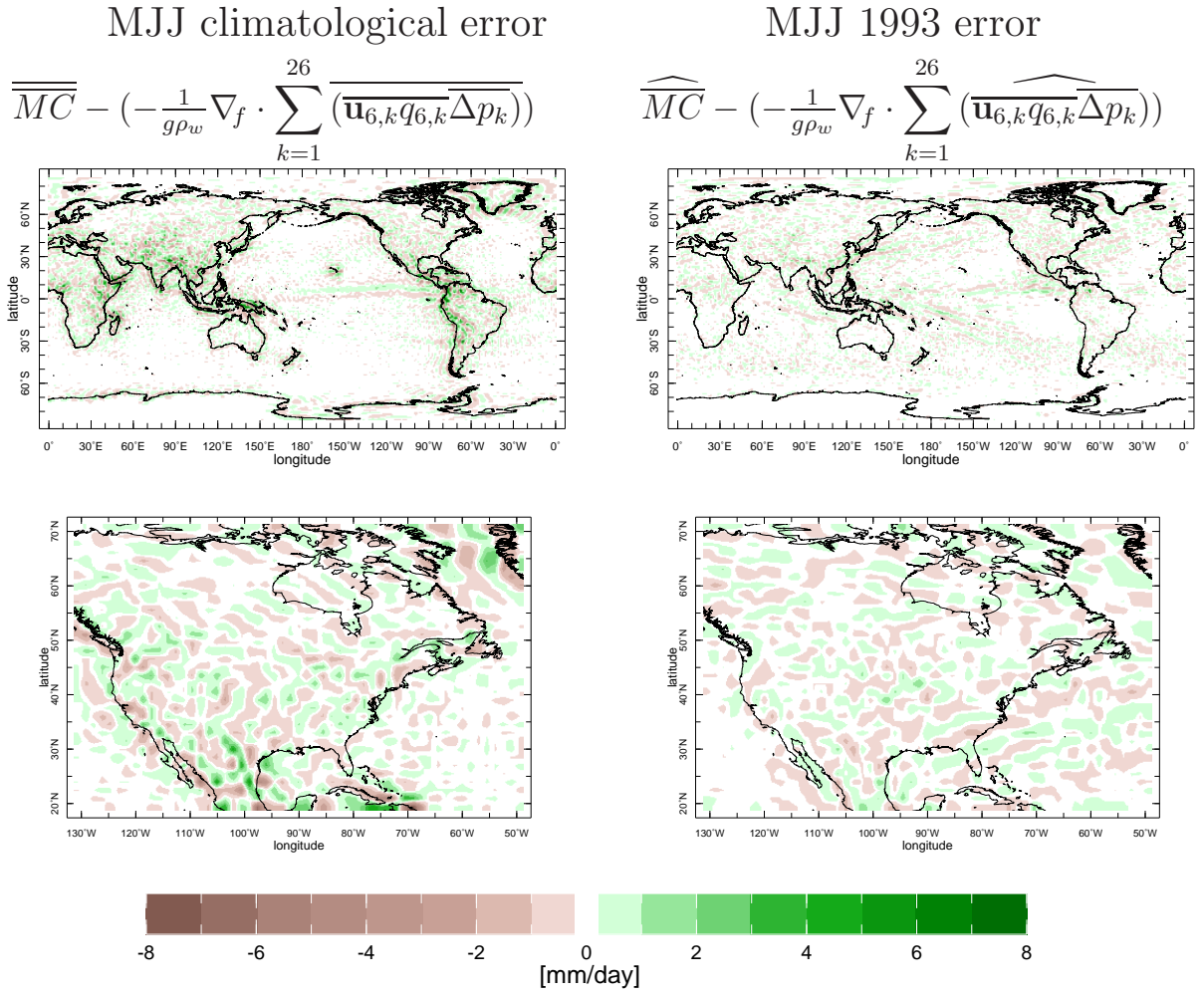


FIG. 9. The difference between ERA-I reported vertically integrated moisture convergence and that computed diagnostically with 6 hourly data on 26 levels for climatological MJJ and just for MJJ 1993 (right) . Units are mm/day

MJJ 1993

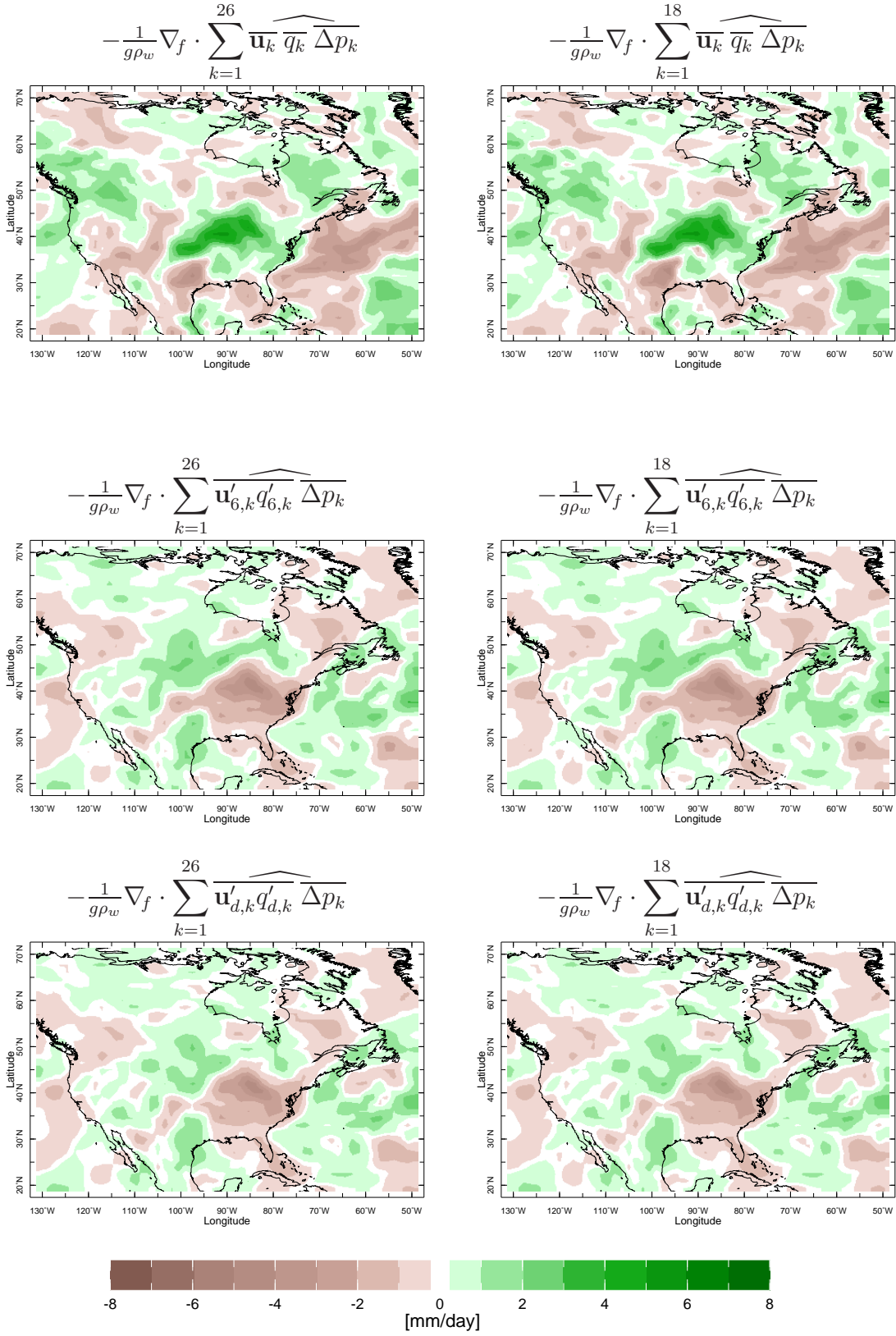
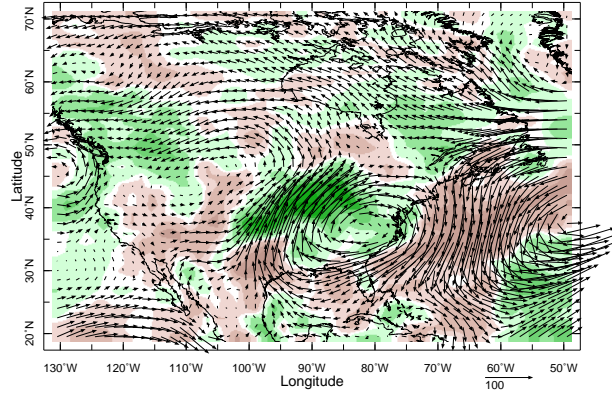


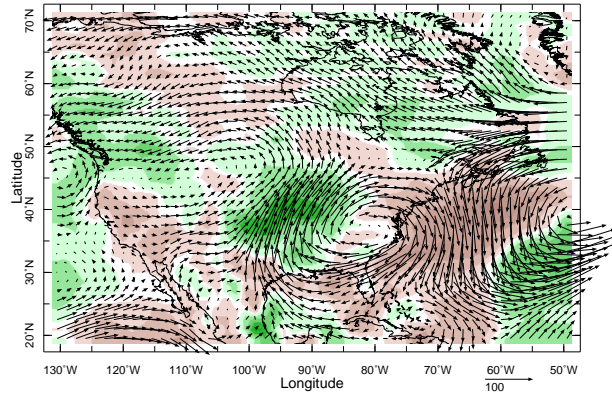
FIG. 10. Components of the MJJ 1993 moisture budget anomaly. The contribution from anomalies in the mean flow and mean humidity evaluated with 26 levels (top left) and 18 levels (top right), the contribution from transient eddy moisture flux convergence evaluated with 6 hourly data (middle) and daily data (bottom) and for 26 levels (left) and 18 levels (right). Units are mm/day

MJJ 1993

$$\frac{1}{g} \sum_{k=1}^{26} \widehat{\mathbf{u}_k} \widehat{q_k} \widehat{\Delta p_k} \text{ and convergence}$$



$$\frac{1}{g} \sum_{k=1}^{26} \widehat{\mathbf{u}_k} \overline{\overline{q_k}} \overline{\overline{\Delta p_k}} \text{ and convergence}$$



$$\frac{1}{g} \sum_{k=1}^{26} \mathbf{u}'_{6,k} \widehat{q'_{6,k}} \overline{\overline{\Delta p_k}} \text{ and convergence}$$

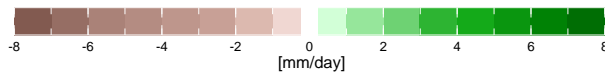
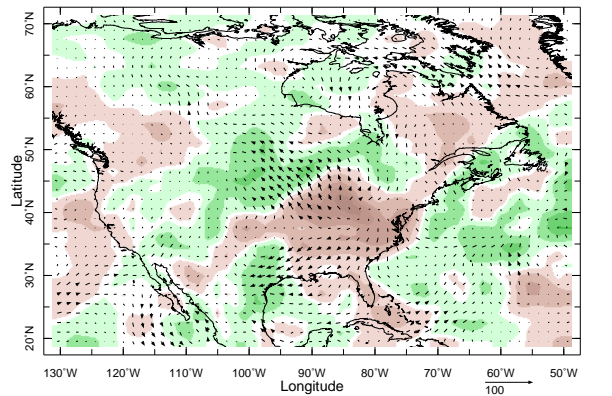


FIG. 11. The MJJ 1993 mean flow moisture flux anomaly and its convergence evaluated with 26 levels (top) and the part of this due to just mean flow anomalies combining with climatological humidity together with its convergence (middle) and the transient eddy moisture fluxes and their convergence evaluated with climatological pressure thicknesses (bottom). Units are $kg/m/s$ for the fluxes and mm/day for the convergence.

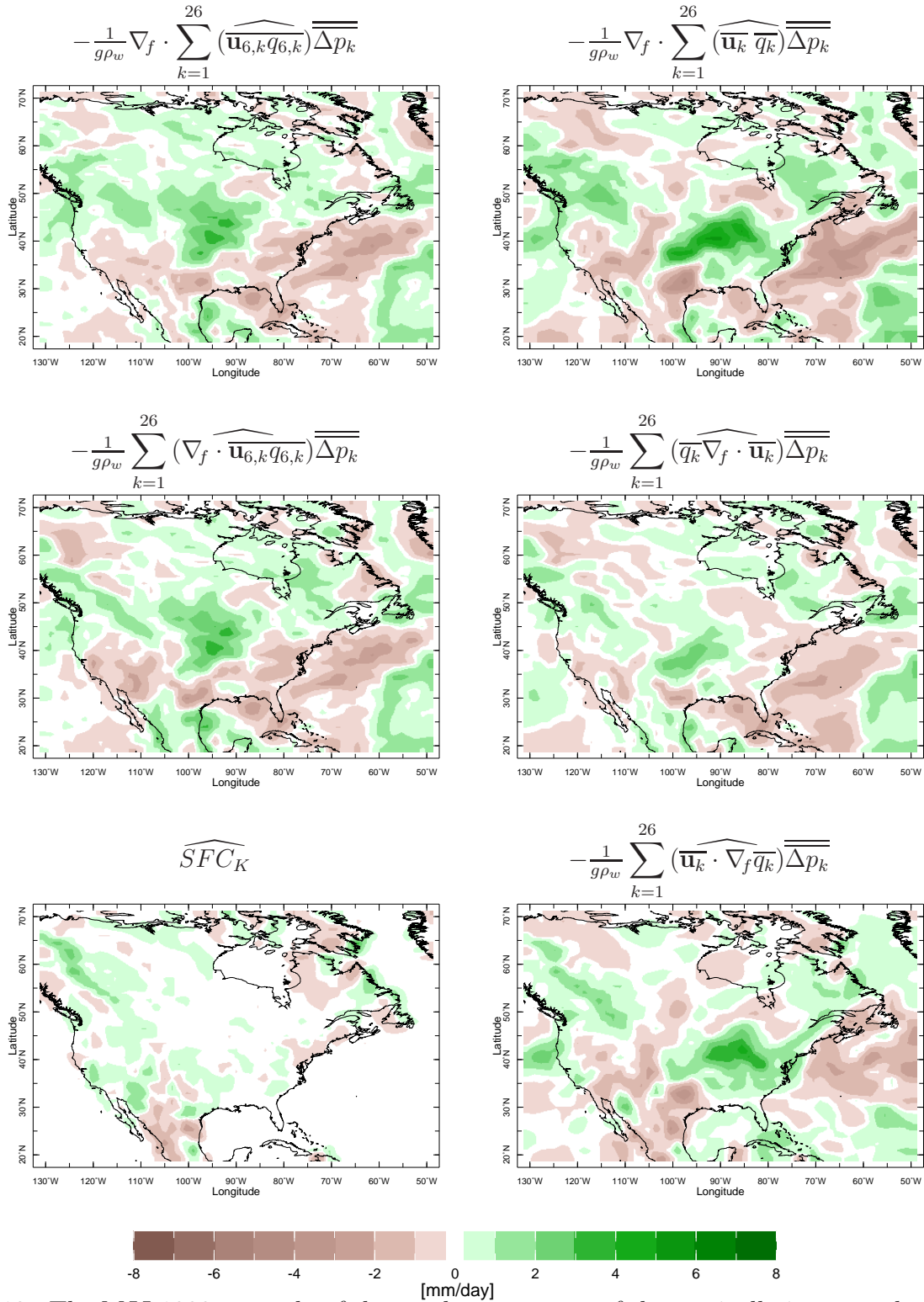
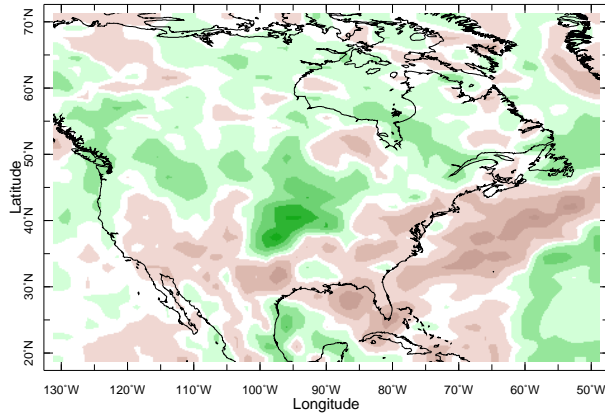


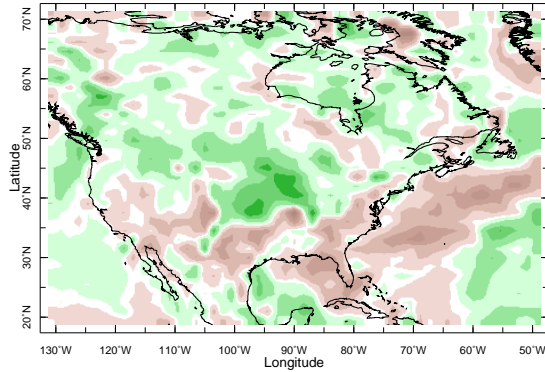
FIG. 12. The MJJ 1993 anomaly of the total convergence of the vertically integrated moisture flux (top left) and its breakdown into the vertical integral of moisture convergence (middle left) and the surface term (bottom left) all using 6 hourly data and 26 levels. The right column shows terms related to the mean flow and mean humidity anomalies. The anomaly of the convergence of vertically integrated mean flow moisture flux (top right), and the components of the vertically integrated moisture convergence due to the mean flow convergence (middle right) and mean flow advection of mean humidity (bottom right). All terms were evaluated using climatological pressure thicknesses. Units are $kg/m/s$ for the fluxes and mm/day for the convergence.

MJJ 1993

$$-\frac{1}{g\rho_w}\nabla_f\cdot\sum_{k=1}^{26}\widehat{(\mathbf{u}_{d,k}q_{d,k}\Delta p_k)}$$



$$-\frac{1}{g\rho_w}\nabla_f\cdot\sum_{k=1}^8\widehat{(\mathbf{u}_{d,k}q_{d,k}\Delta p_k)}$$



$$-\frac{1}{g\rho_w}\nabla_f\cdot\sum_{k=1}^{26}\widehat{(\mathbf{u}_{d,k}q_{d,k}\Delta p_k)} - -\frac{1}{g\rho_w}\nabla_f\cdot\sum_{k=1}^8\widehat{(\mathbf{u}_{d,k}q_{d,k}\Delta p_k)}$$

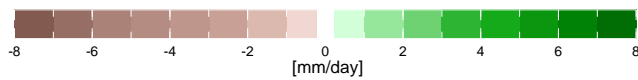
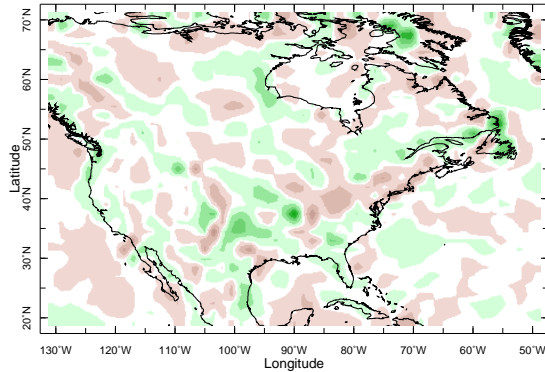


FIG. 13. The MJJ 1993 anomaly of the convergence of the total vertically integrated moisture flux computed with 26 layers (top) and 8 layers (middle) and their difference (bottom). Units are *mm/day*.